

Attention Reallocation: Towards Zero-cost and Controllable Hallucination Mitigation of MLLMs

Chongjun Tu^{1*} Peng Ye^{2,3*} Dongzhan Zhou³ Lei Bai³ Gang Yu⁴ Tao Chen^{1†} Wanli Ouyang^{2,3}

¹ Fudan University ² The Chinese University of Hong Kong ³ Shanghai Artificial Intelligence Laboratory ⁴ StepFun

Abstract

Multi-Modal Large Language Models (MLLMs) stand out in various tasks but still struggle with hallucinations. While recent training-free mitigation methods mostly introduce additional inference overhead via retrospection strategy and contrastive decoding, we propose attention reallocation (AttnReal) to mitigate hallucinations with nearly zero extra cost. Our approach is motivated by the key observations that, MLLM’s unreasonable attention distribution causes features to be dominated by historical output tokens, which further contributes to hallucinated responses because of the distribution gap between different token types. Based on the observations, AttnReal recycles excessive attention from output tokens and reallocates it to visual tokens, which reduces MLLM’s reliance on language priors and ensures the decoding process depends more on the visual inputs. More interestingly, we find that, by controlling the intensity of AttnReal, we can achieve a wide-range trade-off between the response faithfulness and overall performance. Comprehensive results from different benchmarks validate the effectiveness of AttnReal across six open-source MLLMs and three decoding strategies.

1. Introduction

Recently, Multimodal Large Language Models (MLLMs) have achieved remarkable progress, demonstrating superior performance in various tasks like image captioning, visual question answering, and complex content generation (Han et al., 2023; Brooks et al., 2023; Li et al., 2024a;b; Cao et al., 2024; Yang et al., 2024). However, MLLMs encounter a critical challenge known as hallucination, where their responses deviate from the input information, such as describing non-existent objects. Such inaccuracies pose critical risks in safety-sensitive scenarios like autonomous driving (Chen

et al., 2024a; Cui et al., 2024; Shao et al., 2024) and AI-assisted healthcare (He et al., 2023; Wang et al., 2023b; Li et al., 2024a), undermining MLLMs’ reliability.

One effective approach to mitigating hallucinations in MLLMs is fine-tuning the models with carefully curated datasets (Jiang et al., 2024; Wang et al., 2024a; Yin et al., 2024; Li et al., 2024c), which is usually labor-intensive and requires substantial computational resources. Alternatively, training-free methods are proposed to eliminate the need for additional data. Early methods introduce new decoding strategies like Beam Search (Graves, 2012; Sutskever, 2014) and Nucleus Sampling (Holtzman et al., 2019) to increase the likelihood of faithful responses. Recent training-free methods primarily modify the decoding process, applying penalty terms in the beam scores (Huang et al., 2024) or using contrastive decoding (Leng et al., 2024; Liu et al., 2024b; Chuang et al., 2023; Liang et al., 2024) to reduce MLLMs’ over-reliance on statistical biases and language priors, which are regarded as one of the major hallucination origins (Zhou et al., 2023a; Leng et al., 2024; Zhai et al., 2023; Guan et al., 2024). However, these methods require careful design of contrast objects and introduce extra decoding steps, increasing latency and memory overhead. Under such a background, a question naturally arises:

Is it possible to mitigate MLLM hallucinations and improve the performance with nearly zero extra cost, without utilizing additional data or increasing decoding steps?

To answer this question, we investigate the origin of MLLM hallucinations in depth from the perspective of self-attention layers and different token types. We obtain two key observations as follows, which are explained in detail in Section 3.2.

- MLLM’s unreasonable attention allocation between different token types (the input sequence consists of system, visual, instruction, and historical output tokens) gradually amplifies the reliance on language priors, resulting in output tokens dominated features.
- There is a significant gap between the feature distribution of visual tokens and textual tokens, so predicting the next token with features that over-rely on output

*Equal contribution. †Corresponding author.

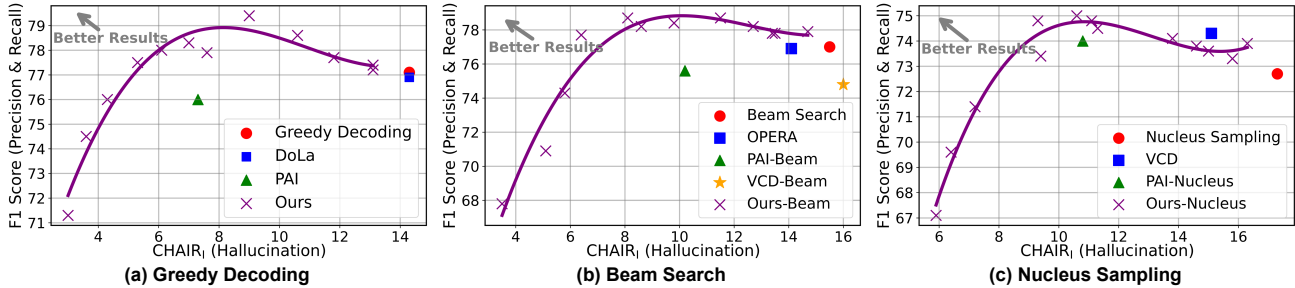


Figure 1: Performance comparison for various training-free methods to mitigate MLLM hallucinations on LLaVA-1.5-7B and the CHAIR benchmark using three decoding strategies. Lower CHAIR₁ represents fewer hallucinations. Higher F1 scores mean better overall performance (precision and recall). The curve in each sub-figure is obtained by adjusting the intensity of our method. Our proposed method not only yields superior results than state-of-the-art methods on different decoding strategies, but also achieves an excellent trade-off between hallucination and F1.

tokens rather than input visual evidence tends to yield hallucinated responses.

Inspired by our findings, we propose a novel attention reallocation (AttnReal) approach, which mitigates hallucinations by redistributing attention values across different token types. Specifically, AttnReal (1) detects and suppresses the attention sinks, which refer to tokens receiving significantly higher attention scores than others, in historical output tokens; (2) reallocates their reduced attention uniformly to visual tokens. AttnReal is plug-and-play and simple-but-effective, demanding no extra data and almost no additional inference or memory overhead. With AttnReal, we suppress the dominance of attention to historical output tokens, ensure decoded features in the forward process are better grounded in visual evidence, and improve the predicted logits, thereby mitigating the hallucinations. Besides, since AttnReal requires only modifications to the attention layers, it can be widely applied to various MLLMs and different decoding strategies. More interestingly, by adjusting the reallocation intensity from the attention sinks to visual tokens, a trade-off between response faithfulness and overall performance can be easily achieved.

Comprehensive results across hallucination benchmarks and GPT-assisted evaluations confirm AttnReal’s effectiveness. As shown in Figure 1, AttnReal achieves a controllable performance trade-off, yielding superior results to the state-of-the-art methods for both faithfulness and F1 scores across a relatively wide range of AttnReal intensities. Moreover, Table 1 compares the decoding overheads of different methods, demonstrating the efficiency advantage of our proposed method. Our contributions can be summarized as follows:

- **The devil of MLLMs’ hallucinations lies in the attention layers.** We investigate the attention and feature distribution from the perspective of self-attention layers, and establish the correlation between MLLM’s unreasonable attention allocation and hallucinations.

Table 1: Decoding overhead comparison among different methods. Greedy refers to the baseline Greedy Decoding. OPERA tracks multiple candidates at every decoding step. VCD, DoLa, and PAI involve contrastive decoding, which introduces additional decoding steps. As a comparison, our proposed method demands minimal extra overhead.

Method	Contrastive Decoding	Candidates per Step	Decoding Overhead (GFLOPs)
Greedy	✗	1	102 / token
OPERA (Huang et al., 2024)	✗	5	1036 / token
VCD (Leng et al., 2024)	✓	1	214 / token
DoLa (Chuang et al., 2023)	✓	1	135 / token
PAI (Liu et al., 2024b)	✓	1	126 / token
Ours	✗	1	104 / token

- **Attention reallocation as a free lunch to reduce MLLM hallucinations.** AttnReal achieves efficient and effective hallucination mitigation by reallocating attention from output sinks to visual tokens. It demands nearly zero extra overhead.
- **Plug-and-play capability and wide applicability.** AttnReal is applied to six open-source MLLMs and three decoding strategies, demonstrating excellent hallucination mitigation performances while improving overall performance under wide ranges of AttnReal intensities.

2. Related Work

2.1. Multi-Modal Large Language Models

Recent advancements in multi-modal large-scale foundation models have greatly improved their cross-modal understanding and generation abilities. Early vision-language models based on BERT (Kenton & Toutanova, 2019) combine visual and textual data to learn image-text interactions. The rise of open-source LLMs, like LLaMA (Touvron et al., 2023a;b) and Vicuna (Chiang et al., 2023), contributes to the development of MLLMs such as LLaVA (Liu et al., 2024a) and MiniGPT-4 (Zhu et al., 2023) that process and generate multi-modal content through instruction tuning. Re-

cent advancements focus on specialized capability enhancements, including spatial grounding (Shikra (Chen et al., 2023)), modular modality collaboration (mPLUG-Owl2 (Ye et al., 2024)), and cross-modal position embedding (Qwen2-VL (Wang et al., 2024b)). Despite these advancements, hallucination remains a persistent challenge across MLLMs. In this paper, we validate the effectiveness of our proposed method on these models.

2.2. Hallucinations in MLLMs

Hallucination and the assessment. MLLM hallucinations refer to generated contents irrelevant or inconsistent with visual inputs, which undermines the models’ reliability and practicality (Yin et al., 2023; Zhou et al., 2023b). Benchmarks like CHAIR (Rohrbach et al., 2018), MMHal-Bench (Sun et al., 2023), and AMBER (Wang et al., 2023a) assess hallucinations by comparing the generated content to the visual inputs and consider metrics like recall and precision to further measure the overall performance. Employing advanced GPT models to assist in evaluations is also a common practice (Huang et al., 2024; Liu et al., 2024b).

Mitigation solutions. Efforts to mitigate MLLM hallucinations can be categorized as training-based and training-free methods. Training-based methods fine-tune models on curated datasets (Liu et al., 2023; Gunjal et al., 2024) or introduce human feedback (Yu et al., 2024), but usually demand significant resources for data annotation and computation. Early training-free methods introduce different decoding strategies, including Beam Search (Boulanger-Lewandowski et al., 2013), which tracks multiple candidate sequences, and Nucleus Sampling (Holtzman et al., 2019) that emphasizes coherent and varied outputs. To further mitigate hallucinations, which are found to be associated with MLLM’s over-reliance on statistical bias and language priors (Yue et al., 2024), various improvements have been proposed recently. OPERA (Huang et al., 2024) improves Beam Search with a penalty term in the beam scores as well as a retrospection strategy. Other studies apply contrastive decoding to calibrate the MLLM’s predicted logits: DoLa (Chuang et al., 2023) compares layer-wise predictions, HALC (Chen et al., 2024b) compares predictions between visual context windows, VCD (Leng et al., 2024) and PAI (Liu et al., 2024b) construct contrastive inputs by distorting and removing the input images, respectively. While training-free, these methods incur inference overhead from tracking several candidates or multiple decoding steps. In contrast, our proposed AttnReal suppresses hallucinations within a single forward pass, eliminating additional memory overhead and inference latency. Moreover, our method allows for a wide-range controllable trade-off between response faithfulness and overall performance, catering to different application scenarios.

2.3. Attention Mechanism about MLLM Hallucinations

Recent studies have made progress on the attention mechanism of MLLMs. Researchers develop new attention mechanisms and fine-tune MLLMs to suppress the diminishing attention scores between distant visual cues and output tokens due to Rotary Position Embeddings (RoPE), mitigating hallucinations (Ma et al., 2024; Xing et al., 2024). Meanwhile, the attention sink phenomenon (Xiao et al., 2023; Huang et al., 2024) has been observed, which refers to tokens receiving significantly higher attention scores than others but providing limited semantic information. Distinct from these studies, we explore the attention allocation as well as the feature distribution between different token types rather than the token-level mechanism. Besides, we establish the correlation between our observation and hallucinations, based on which we introduce a training-free mitigation solution.

3. Method

3.1. Preliminaries

In this section, we formulate the MLLM decoding process to facilitate an easier understanding of the proposed attention reallocation method.

Input organization. Most existing MLLMs transform the input contents into token sequences and organize them in the order of system tokens, visual tokens, and instruction tokens. In the auto-regressive decoding process, models concatenate the historically generated output tokens to the post of the initial input token sequence. Thus, the input sequence of the model can be denoted as $[X_s, X_v, X_i, X_o]$ except for the generation of the first token.

Forward process. The input token sequence is fed through multiple transformer layers to obtain the final hidden states. For a given input sequence with n tokens $\mathbf{X} = [X_s, X_v, X_i, X_o]$ to a specific layer, the model generates the output hidden states as follows:

$$h = Af_V(\mathbf{X}), A = \text{Softmax}\left(\frac{f_Q(\mathbf{X})f_K(\mathbf{X})^T}{\sqrt{d_k}}\right), \quad (1)$$

where f_Q , f_K , and f_V are the projection matrices for the queries, keys, and values, d_k denotes the embedding dimensions and h represents the output hidden states. The attention matrix $A \in \mathbb{R}^{n \times n}$ can be decomposed into matrices for each token type: $A = [A_s, A_v, A_i, A_o]$. Similarly, the value matrix $V = f_V(\mathbf{X}) \in \mathbb{R}^{n \times d_k}$ can also be decomposed based on token type: $V = [V_s, V_v, V_i, V_o]^T$. Therefore, the output hidden states can be reformulated as:

$$h = A_sV_s + A_vV_v + A_iV_i + A_oV_o. \quad (2)$$

Based on Equation (2), we can regard the attention to different token types as the weights of tokens during the feature mixing for the output feature, which enables MLLMs to gather information from different token representations.

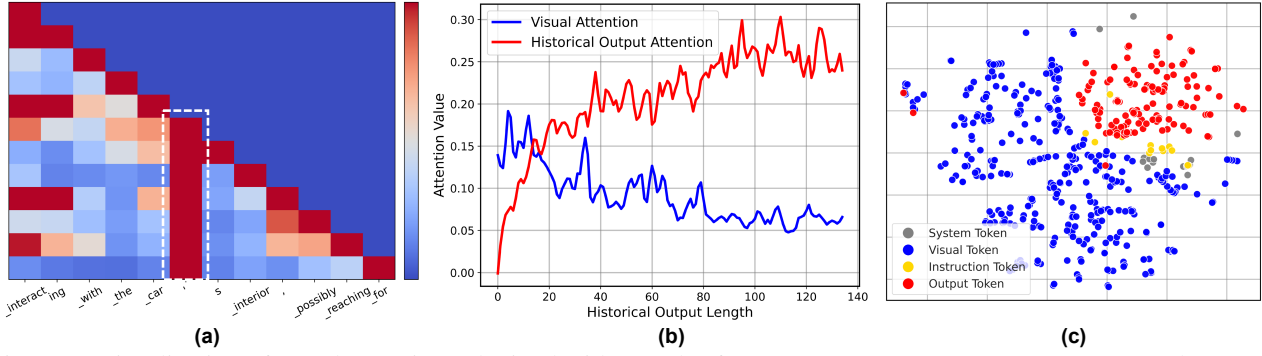


Figure 2: Visualization of our observations obtained with samples from MSCOCO on Qwen2-VL (Wang et al., 2024b). (a) A case of the attention sink phenomenon among output tokens. Red areas represent high attention values. The words corresponding to each token are shown below each column. (b) Changes in MLLM’s total attention value to historical output tokens and visual tokens. (c) Visualization of feature distribution of different tokens in the last decoder layer of the MLLM.

Next token prediction. The output hidden states of the last layer h are projected using a vocabulary head \mathcal{H} to obtain predicted logits for the next token:

$$\text{logits} = \text{Softmax}(\mathcal{H}(h)), \quad (3)$$

where $\text{logits} \in \mathbb{R}^v$ and v is the vocabulary set size.

3.2. Observations

One of the major origins of hallucinations in MLLMs lies in their over-reliance on language priors (Leng et al., 2024; Yue et al., 2024). However, how this over-reliance manifests during the decoding process and how it contributes to hallucinated responses remain under-explored. In this section, we conduct in-depth exploratory experiments from the perspective of the self-attention layers and token types, considering that MLLM decoding involves various types of tokens. Our observations are as follows.

MLLM’s unreasonable attention allocation gradually amplifies language prior reliance, which leads to output token dominated features. As evidenced by Equation (2), the output hidden states are obtained by weighing features of different token types using attention values. Therefore, we visualize the changes in MLLM’s attention to different token types as the length of the historical output token increases. Specifically, for each generated token, we sum the post-softmax attention values received by each token type and average these sums across all MLLM layers to obtain the results. As can be concluded from sub-figure (b) of Figure 2, the attention allocated for historical output tokens gradually rises, while visual attention declines, i.e., A_o is increasing and A_v is decreasing in Equation (2). Therefore, this attention allocation pattern reveals that the MLLM gradually relies more on language priors, and the features are gradually dominated by output tokens, especially when the output sequence gets longer.

The evident distribution gap between different token types translates output token dominance into halluci-

nated responses. To further bridge the correlation between features dominated by historical output tokens and hallucinations, we visualize and analyze the feature distributions of different token types in the last decoder layer of the MLLM. As can be observed from sub-figure (c) in Figure 2, there exists a significant distribution gap between visual tokens and textual tokens (including system, instruction, and output tokens). Since the decoded features are gradually dominated by historical output tokens, the next token tends to distribute closer to textual token embeddings while deviating from visual features. When decoding with the visually ungrounded features, the logits of next-token predictions become susceptible to statistical biases from the LLM pretraining process and tend to yield textually coherent but visually irrelevant tokens (e.g., inferring “people” when only a car is visible), resulting in hallucinated responses.

3.3. Attention Reallocation

We have revealed that unreasonable attention allocation is an important origin of MLLM hallucinations in Section 3.2. Therefore, in this section, we propose the attention reallocation (**AttnReal**) approach with almost zero additional cost to effectively mitigate MLLM hallucinations and improve the consistency of the predicted results with the input visual evidence. Specifically, AttnReal comprises two steps: attention recycling and attention allocation.

Step 1: attention recycling. To avoid MLLMs from relying unreasonably heavily on historical output tokens during the decoding process, we first recycle the attention allocated to output tokens in self-attention layers. According to the attention sink phenomenon (Xiao et al., 2023; Huang et al., 2024), there exist some tokens that receive significantly high attention scores but provide limited semantic information among the output tokens (visualized in subfigure (a) of Figure 2). Based on this phenomenon, we focus on recycling attention from these attention sinks to suppress the dominance of output tokens. Denote the current input token sequence as $[X_s, X_v, X_i, X_o]$ and the corresponding attention map after softmax as $[A_s, A_v, A_i, A_o]$. We identify the

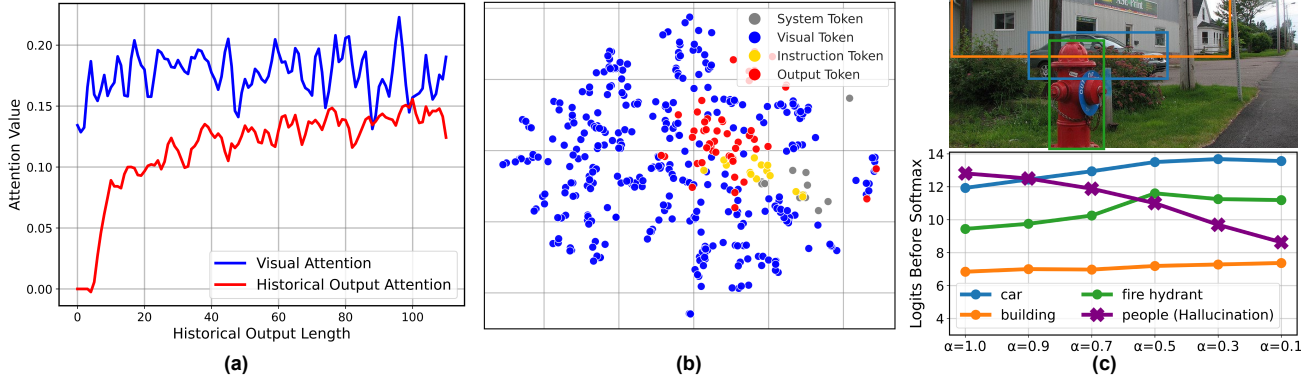


Figure 3: (a) Changes in MLLM’s total attention value to historical output tokens and visual tokens when applying our AttnReal. (b) Feature distribution of different tokens in the last decoder layer of the MLLM when applying our AttnReal. (c) The upper part shows the image provided to the MLLM, in which the ground-truth objects are highlighted with different colors. The lower part demonstrates the MLLM’s predicted logits for various tokens at different intensities of our AttnReal.

attention sinks in the output tokens X_o by setting a sink threshold \mathcal{T} . The identified attention sink set is as follows:

$$S_{sink} = \{x_j \mid a_j > \mathcal{T} \cdot \frac{1}{n}\}, \text{ for } x_j \in X_o, j = 1, \dots, n_o, \quad (4)$$

where $a_j \in A_o$ is the corresponding attention score to x_j . n denotes the input sequence length, and n_o is the number of output tokens. This equation defines attention sinks to be output tokens receiving more than \mathcal{T} times the average attention score, i.e., $\frac{1}{n}$. Next, we introduce a down-scaling factor α for attention recycling, whose value determines the intensity of AttnReal. Specifically, the attention scores $a_j \in A_o$ are updated as follows:

$$a'_j = \begin{cases} \alpha \cdot a_j, & \text{if } x_j \in S_{sink}, \\ a_j, & \text{if } x_j \notin S_{sink}, \end{cases} \text{ for } j = 1, \dots, n_o. \quad (5)$$

Step 2: attention allocation. To utilize the recycled attention to effectively reduce MLLM’s hallucinations, we allocate it to visual tokens, enhancing the alignment between the output hidden states and visual features. Denote the reduction of attention to output tokens as Δ_{A_o} and the number of visual tokens as n_v . We uniformly allocate the attention to visual tokens $a_k \in A_v$, which can be formulated as:

$$a'_k = a_k + \frac{\Delta_{A_o}}{n_v}, \quad k = 1, \dots, n_v. \quad (6)$$

This allocation process increases the MLLM’s awareness of the visual information and yields output hidden states better aligned with the visual embeddings. Overall, AttnReal reallocates the attention values, contributing to better output hidden states and predicted logits, ultimately reducing hallucinations in MLLMs.

3.4. Effectiveness of Attention Reallocation

To examine whether AttnReal works as expected, we visualize the attention value and feature distribution of different token types when AttnReal is applied. As shown in sub-figure (a) of Figure 3, MLLM’s attention to the visual tokens

remains broadly stable with fluctuations, while the attention to output tokens grows slightly but stays lower than the visual tokens. Sub-figure (b) demonstrates that by applying AttnReal, the MLLM achieves better alignment between output features and input visual features, contributing to predictions that are more grounded in the visual embeddings.

Furthermore, we compare the changes of predicted logits at varying down-scaling factors α in sub-figure (c) of Figure 3 to provide further evidence about how AttnReal reduces hallucinations. Specifically, given the upper image of sub-figure (c), the MLLM is asked to generate a description. The results of $\alpha = 1.0$ in the lower part of sub-figure (c) correspond to the baseline, in which the hallucination token “people” achieves the highest logits and is generated, although there does not exist any person in the image. As we increase the intensity of AttnReal, i.e., reduce the value of α , the logits of “people” gradually decrease, and the logits of ground-truth tokens like “car” and “building” increase. When $\alpha = 0.7$, the logits of “car” surpass that of “people” and the hallucination is eliminated.

4. Experiments

4.1. Setup

Baselines. In this paper, we choose six representative MLLM backbones to validate the plug-and-play effectiveness of our proposed AttnReal approach, including LLaVA-1.5-7B (Liu et al., 2024a), LLaVA-1.5-13B, MiniGPT-4 (Zhu et al., 2023), Shikra (Chen et al., 2023), mPLUG-Owl2 (Ye et al., 2024), and Qwen2-VL (Wang et al., 2024b). These models are 7B models except for LLaVA-1.5-13B. Moreover, to show the wide applicability, we apply AttnReal to three decoding strategies: Greedy Decoding, Beam Search, and Nucleus Sampling. For performance comparisons, we focus on training-free methods for MLLM hallucination mitigation, including DoLa (Chuang et al., 2023),

Table 2: CHAIR evaluation results on five open-source MLLMs. CHAIR_S and CHAIR_I (lower is better) reflect the degree of hallucination. The F1 score (higher is better) represents the comprehensive consideration of accuracy and recall. In *CHAIR-aligned* lines, we align CHAIR_S and CHAIR_I with the best hallucination performance of other methods and focus on the F1 score comparison. In *F1-aligned* lines, we align our F1 score with the highest F1 of other methods and emphasize the improvements in CHAIR metrics. “-” means the corresponding method is not implemented in this model.

Methods	Decoding Strategy	LLaVA-1.5-7B			LLaVA-1.5-13B			MiniGPT-4		
		CHAIR _S ↓	CHAIR _I ↓	F1 ↑	CHAIR _S ↓	CHAIR _I ↓	F1 ↑	CHAIR _S ↓	CHAIR _I ↓	F1 ↑
Greedy		47.0	14.3	77.1	44.8	12.8	77.9	31.0	9.6	70.6
DoLa (Chuang et al., 2023)		46.8	14.3	76.9	-	-	-	29.2	10.1	71.5
PAI (Liu et al., 2024b)	Greedy Decoding	29.6	7.3	76.0	35.6	9.2	77.9	24.4	9.0	70.9
Ours (CHAIR-aligned)		30.6	7.0	78.3 (↑1.2)	36.6	8.7	79.7 (↑1.8)	25.6	7.7	70.9
Ours (F1-aligned)		23.0 (↓6.6)	5.3 (↓1.7)	77.3	24.6 (↓11.0)	5.0 (↓4.2)	78.0	27.8	8.2 (↓0.8)	71.5
Beam Search		51.8	15.5	77.0	49.0	13.4	78.3	34.4	10.9	70.4
OPERA (Huang et al., 2024)		48.6	14.1	76.9	40.4	12.4	76.8	28.6	10.1	69.6
VCD-Beam (Leng et al., 2024)		52.6	16.0	74.8	48.4	14.5	75.0	32.4	9.8	69.8
PAI-Beam (Liu et al., 2024b)	Beam Search	35.0	10.2	75.6	40.4	12.6	77.0	24.0	8.7	69.8
Ours-Beam (CHAIR-aligned)		36.6	9.8	78.4 (↑1.4)	40.0	9.6	79.5 (↑1.2)	24.2	6.7	71.4 (↑1.0)
Ours-Beam (F1-aligned)		21.6 (↓13.4)	6.4 (↓3.8)	77.4	27.8 (↓12.6)	6.5 (↓6.1)	78.5	17.2 (↓6.8)	5.5 (↓3.2)	70.3
Nucleus Sampling		52.8	17.3	72.7	54.2	15.6	73.8	34.6	11.0	69.5
VCD (Leng et al., 2024)		48.4	15.1	74.3	50.0	14.5	76.0	32.0	10.3	68.8
PAI-Nucleus (Liu et al., 2024b)	Nucleus Sampling	39.2	10.8	74.0	41.0	12.8	76.1	23.2	9.2	70.9
Ours-Nucleus (CHAIR-aligned)		42.0	10.6	75.0 (↑0.7)	42.6	10.1	77.6 (↑1.5)	25.4	7.6	70.0
Ours-Nucleus (F1-aligned)		42.2	9.3 (↓1.5)	74.8	37.2 (↓3.8)	7.9 (↓4.9)	76.2	26.0	9.9	70.5

Methods	Decoding Strategy	Shikra			mPLUG-Owl2		
		CHAIR _S ↓	CHAIR _I ↓	F1 ↑	CHAIR _S ↓	CHAIR _I ↓	F1 ↑
Greedy		56.6	16.4	74.5	59.0	19.3	71.1
DoLa (Chuang et al., 2023)		-	-	-	58.2	18.6	71.5
PAI (Liu et al., 2024b)	Greedy Decoding	31	8.6	74.9	-	-	-
Ours (CHAIR-aligned)		31.2	7.6	75.6 (↑0.7)	37.0	11.1	75.3 (↑3.8)
Ours (F1-aligned)		24.2 (↓6.8)	5.9 (↓2.7)	75.3	19.8 (↓38.4)	6.2 (↓12.4)	72.9
Beam Search		57.0	15.5	75.1	58.2	18.1	73.1
OPERA (Huang et al., 2024)		38.4	12.9	73.8	50.8	16.9	72.2
VCD-Beam (Leng et al., 2024)		-	-	-	59.6	19.9	68.8
PAI-Beam (Liu et al., 2024b)	Beam Search	33.8	10.0	74.5	-	-	-
Ours-Beam (CHAIR-aligned)		34.2	8.1	77.0 (↑1.9)	43.0	13.6	75.2 (↑2.1)
Ours-Beam (F1-aligned)		21.8 (↓12.0)	5.2 (↓4.8)	75.1	22.8 (↓28.0)	7.9 (↓9.0)	73.2
Nucleus Sampling		60.8	16.1	72.5	61.2	19.8	68.9
VCD (Leng et al., 2024)		-	-	-	58.4	20.3	68.9
PAI-Nucleus (Liu et al., 2024b)	Nucleus Sampling	34.2	8.9	74.1	-	-	-
Ours-Nucleus (CHAIR-aligned)		36.6	7.9	76.6 (↑2.5)	36.8	11.4	72.3 (↑3.4)
Ours-Nucleus (F1-aligned)		33.0 (↓1.2)	7.1 (↓1.8)	74.2	28.6 (↓29.8)	9.0 (↓11.3)	70.4

Table 3: CHAIR evaluation results on Qwen2-VL (Wang et al., 2024b). CHAIR_S and CHAIR_I reflect the degree of hallucination, and the F1 score represents the comprehensive consideration of accuracy and recall.

Methods	Decoding Strategy	Qwen2-VL		
		CHAIR _S ↓	CHAIR _I ↓	F1 ↑
Greedy		30.0	8.9	77.1
Ours (CHAIR-aligned)	Greedy Decoding	25.8	7.8	78.3 (↑1.2)
Ours (F1-aligned)		21.0 (↓9.0)	5.9 (↓3.0)	77.1

OPERA (Huang et al., 2024), VCD (Leng et al., 2024), and PAI (Liu et al., 2024b). DoLa is applied to Greedy Decoding by default. OPERA relies on Beam Search. VCD is based on Nucleus Sampling and can be applied with Beam Search. PAI can be adopted with all three decoding strategies. All baselines are implemented with the default hyperparameters from their open-source codes.

Implementation details. All compared methods are evaluated with the same random seed and decoding strategy settings. For Beam Search, the number of beam candi-

dates is set to 5, and for Nucleus Sampling the common parameters are consistent. For AttnReal, we set the sink threshold $\mathcal{T} = 1$ for all MLLMs by default unless otherwise stated, given that the attention value of most tokens is much smaller than the average due to attention sinks. Moreover, AttnReal is robust to different \mathcal{T} values, as demonstrated in Section 4.3.

4.2. Quantitative Results

In this section, we evaluate the performance of AttnReal with MLLM hallucination evaluation benchmarks and GPT-assisted open evaluation, covering evaluations for various hallucination types and overall performance.

4.2.1. CHAIR EVALUATION

Caption Hallucination Assessment with Image Relevance (CHAIR) (Rohrbach et al., 2018) is a specifically crafted benchmark to assess object hallucination in the image cap-

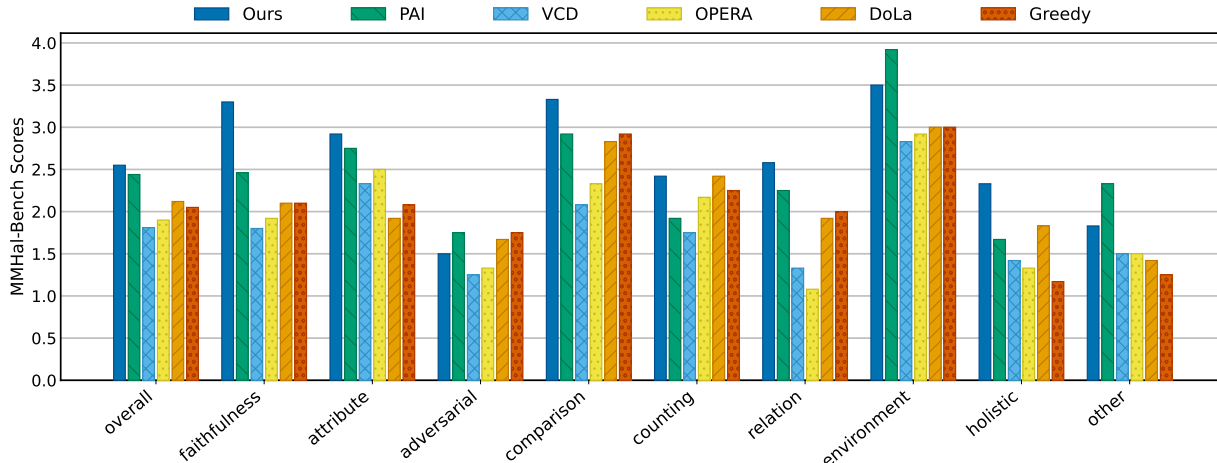


Figure 4: Comparative results on the MMHal-Bench and LLaVA-1.5-7B. To all metrics, higher scores mean better performance.

tioning task. Specifically, CHAIR provides the ground-truth object labels for all samples and evaluates hallucinations in given image descriptions by calculating the ratio of all objects mentioned in the description that are not present in the ground-truth label set. CHAIR comprises two quantitative metrics, CHAIR_S and CHAIR_I, to assess the sentence-level and instance-level hallucination, respectively. Besides hallucination metrics, we also adopt the F1 score, which is decided by both precision and recall, to evaluate the overall performance. We follow the settings of (Huang et al., 2024; Liu et al., 2024b) to perform CHAIR evaluation on the validation set of MSCOCO 2014 (Lin et al., 2014). Specifically, we randomly sample 500 samples from the validation set and prompt the MLLMs with "Please describe this image in detail." for caption generation, with the *max_new_tokens* parameter set to 512.

Results of CHAIR. Tables 2 and 3 exhibit the comprehensive results of different methods on 6 MLLMs and 3 decoding strategies. Since our proposed AttnReal achieves a wide-range trade-off between CHAIR metrics and F1 scores, as illustrated in Figure 1, we show our performances under two settings: 1) We align the hallucination performance (CHAIR_S and CHAIR_I) with the lowest CHAIR metrics of existing methods and compare the F1 scores. 2) We also align the F1 performance with the best of other methods and compare the CHAIR metrics. From Table 2 we can conclude that for most MLLMs and decoding strategies, our proposed method achieves higher F1 scores with aligned CHAIR metrics and yields lower hallucinations with aligned F1, demonstrating its effectiveness and wide applicability. For Qwen2-VL (Wang et al., 2024b), which has not been integrated by existing studies, we enhance the F1 score from 77.1 to 78.3 with lower hallucination, and reduce the CHAIR_S/CHAIR_I metrics from 30.0 / 8.9 to 21.0 / 5.9 with aligned F1 score. More results on the CHAIR benchmark

are provided in Appendix A.1 of the appendix.

4.2.2. MMHAL-BENCH

MMHal-Bench (Sun et al., 2023) is a challenging benchmark to evaluate the model’s comprehensive performance across various hallucination types. It consists of 96 samples that are evenly distributed across 8 different hallucination types, including object attributes, adversarial objects, comparisons, counting, spatial relations, environment, holistic descriptions, and other hallucinations. For the model’s responses, MMHal-Bench uses GPT-4 to compare them with carefully crafted ground-truth answers and rates the output for each sample between 0-6 depending on three aspects: informativeness, hallucination, and logical analysis. The evaluation results include the overall score and hallucination rate on all samples, as well as ratings for each hallucination type. We convert the hallucination rate into a faithfulness rate and scale it to a score between 0-6 as an overall faithfulness score to display together with other ratings.

Results of MMHal-Bench. In Figure 4, we show the comparative results of various methods on the MMHal-Bench and LLaVA-1.5-7B. Our proposed AttnReal method achieves the best overall performance and significantly enhances the faithfulness scores compared to existing methods. Besides, AttnReal receives the highest ratings on 5 out of 8 hallucination types and gains improvement on 7 of 8 hallucination types compared to Greedy Decoding, exhibiting strong competitiveness. Please refer to Appendix A.5 in the appendix for the results of other MLLMs on MMHal-Bench.

4.2.3. GPT-ASSISTED EVALUATION

We further rely on GPT-4o, a strong multi-modal assistant, to conduct the open evaluation of MLLMs’ output quality. Compared to CHAIR (Rohrbach et al., 2018), GPT-assisted

Table 4: Quantitative comparison on GPT-assisted evaluation. The best results are **bolded**, and the suboptimal results are underlined. \mathcal{C} and \mathcal{D} represent for correctness and detailedness, respectively. “-” means the corresponding method is not implemented in this model.

Method	LLaVA-1.5-7B		LLaVA-1.5-13B		MiniGPT-4		Shikra		mPLUG-Owl2		Qwen2-VL	
	\mathcal{C}	\mathcal{D}										
Greedy	3.22	3.35	3.38	3.43	2.80	3.25	2.99	3.23	2.66	3.10	<u>4.08</u>	<u>3.93</u>
DoLa (Chuang et al., 2023)	3.25	<u>3.41</u>	-	-	2.81	3.21	-	-	<u>2.67</u>	3.08	-	-
OPERA (Huang et al., 2024)	<u>3.31</u>	<u>3.41</u>	3.36	3.37	3.03	3.22	3.02	3.14	2.65	3.07	-	-
VCD (Leng et al., 2024)	3.15	3.32	3.18	3.34	2.88	3.22	-	-	2.56	3.00	-	-
PAI (Liu et al., 2024b)	3.24	3.29	<u>3.40</u>	<u>3.53</u>	3.13	3.36	<u>3.13</u>	<u>3.28</u>	-	-	-	-
Ours	3.40	3.44	3.47	3.55	<u>3.07</u>	<u>3.35</u>	3.14	3.36	3.04	3.36	4.17	3.97

evaluation provides more assessments beyond object hallucination. We follow (Huang et al., 2024; Liu et al., 2024b; Leng et al., 2024) to randomly select 500 samples from the validation set of MSCOCO and ask MLLMs to generate corresponding descriptions. Then we provide the responses along with the images to GPT-4o, prompting it to rate the correctness (\mathcal{C}) and detailedness (\mathcal{D}) of each output from 0-5 respectively. Please refer to Appendix C in the appendix for detailed prompts used in this section.

Results of GPT-assisted evaluation. Quantitative comparison of various methods on GPT-assisted evaluation is provided in Table 4. Our proposed method yields both the best correctness scores and the best detailedness scores on most MLLMs. This means that when integrated with our proposed method, MLLMs can generate more precise responses without sacrificing the details in the input images.

4.3. Ablation Study

Our proposed AttnReal first identifies and suppresses attention sinks in the historical output tokens and then reallocates the reduced attention to visual tokens. This process involves two hyper-parameters in total: the sink threshold \mathcal{T} and down-scaling factor α . We select LLaVA-1.5-7B as the representative MLLM to examine the impact of different hyper-parameters on the performance. The ablation study is conducted on the CHAIR benchmark, and the generated responses are evaluated with both CHAIR metrics and the F1 score. For a given sink threshold \mathcal{T} , we can adjust the intensity of AttnReal, achieving a wide-range trade-off between response faithfulness and overall performance through α , as illustrated in Figure 1.

We further explore the impact of different \mathcal{T} values on the performance. Specifically, we selected four values with large differences to demonstrate the robustness of AttnReal to sink threshold configurations, i.e., $\mathcal{T} = [0.1, 1, 10, 100]$. As can be concluded from Figure 5, the results of different settings show a consistent tendency. As α decreases from 1, the CHAIR metrics gradually reduce from the baseline, representing decreased hallucinations. The F1 score first rises with the intensity of AttnReal and begins to drop when

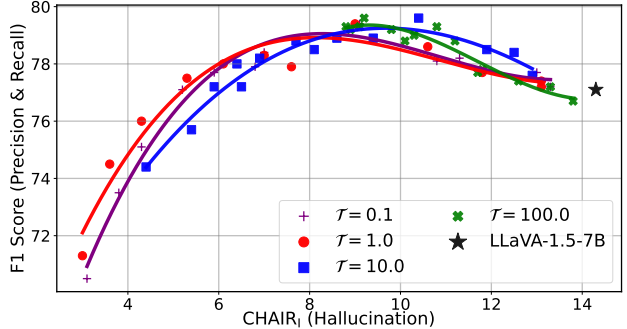


Figure 5: Ablation study on LLaVA-1.5-7B about the effect of different sink thresholds \mathcal{T} on the performance.

the hallucinations have been significantly suppressed. This change is because the F1 score is determined by both precision and recall. With lower intensities of AttnReal, there is an evident improvement in precision, which leads to a higher F1 score. However, when the intensity of AttnReal is high, there are fewer hallucinations, and it is difficult to further improve the precision. At this point, the MLLM tends to focus on the most prominent visual features and may discard some tokens with less certainty, which leads to a lower recall and a subsequent decline in the F1 score.

5. Conclusion

In this paper, we observe that unreasonable attention allocation in MLLMs causes features to be dominated by historical output tokens, leading to hallucinated responses due to feature gaps between visual and output tokens. To address this, we propose a nearly zero-cost method called attention reallocation (AttnReal), reducing excessive attention to output tokens and encouraging MLLM to rely more on visual evidence. By adjusting the down-scaling factor of AttnReal, we can balance response faithfulness and overall performance as needed. Evaluations across various MLLMs and decoding strategies verify the effectiveness of AttnReal. The limitation of our work is that AttnReal relies on historical output tokens and is not well-suited to addressing hallucinations in tasks with particularly short responses. Besides, it is worth investigating how to extend the zero-cost hallucination mitigation solution to more tasks and models.

Impact Statement

This paper introduces AttnReal, a training-free approach to effectively mitigate hallucinations in Multimodal Large Language Models (MLLMs) with nearly zero extra overhead.

By redistributing attention values during the decoding process, AttnReal can significantly enhance MLLMs’ response faithfulness and reliability in safety-critical applications such as autonomous driving and healthcare, where hallucinated responses could lead to severe consequences.

Besides, AttnReal requires no additional training data, avoids costly fine-tuning, and eliminates extra inference latency introduced by methods of multiple decoding steps. This efficiency reduces computational resource consumption and lowers the carbon footprint associated with training and deploying MLLMs.

References

- Boulanger-Lewandowski, N., Bengio, Y., and Vincent, P. Audio chord recognition with recurrent neural networks. In *ISMIR*, pp. 335–340. Curitiba, 2013.
- Brooks, T., Holynski, A., and Efros, A. A. Instructpix2pix: Learning to follow image editing instructions. In *Proceedings of the IEEE/CVF Conference on Computer Vision and Pattern Recognition*, pp. 18392–18402, 2023.
- Cao, J., Ye, P., Li, S., Yu, C., Tang, Y., Lu, J., and Chen, T. Madtp: Multimodal alignment-guided dynamic token pruning for accelerating vision-language transformer. In *Proceedings of the IEEE/CVF Conference on Computer Vision and Pattern Recognition*, pp. 15710–15719, 2024.
- Chen, K., Zhang, Z., Zeng, W., Zhang, R., Zhu, F., and Zhao, R. Shikra: Unleashing multimodal llm’s referential dialogue magic. *arXiv preprint arXiv:2306.15195*, 2023.
- Chen, L., Sinavski, O., Hünermann, J., Karnsund, A., Willmott, A. J., Birch, D., Maund, D., and Shotton, J. Driving with llms: Fusing object-level vector modality for explainable autonomous driving. In *2024 IEEE International Conference on Robotics and Automation (ICRA)*, pp. 14093–14100. IEEE, 2024a.
- Chen, Z., Zhao, Z., Luo, H., Yao, H., Li, B., and Zhou, J. Halc: Object hallucination reduction via adaptive focal-contrast decoding. *arXiv preprint arXiv:2403.00425*, 2024b.
- Chiang, W.-L., Li, Z., Lin, Z., Sheng, Y., Wu, Z., Zhang, H., Zheng, L., Zhuang, S., Zhuang, Y., Gonzalez, J. E., et al. Vicuna: An open-source chatbot impressing gpt-4 with 90%* chatgpt quality. See <https://vicuna.lmsys.org> (accessed 14 April 2023), 2(3):6, 2023.
- Chuang, Y.-S., Xie, Y., Luo, H., Kim, Y., Glass, J., and He, P. Dola: Decoding by contrasting layers improves factuality in large language models. *arXiv preprint arXiv:2309.03883*, 2023.
- Cui, C., Ma, Y., Cao, X., Ye, W., Zhou, Y., Liang, K., Chen, J., Lu, J., Yang, Z., Liao, K.-D., et al. A survey on multimodal large language models for autonomous driving. In *Proceedings of the IEEE/CVF Winter Conference on Applications of Computer Vision*, pp. 958–979, 2024.
- Graves, A. Sequence transduction with recurrent neural networks. *arXiv preprint arXiv:1211.3711*, 2012.
- Guan, T., Liu, F., Wu, X., Xian, R., Li, Z., Liu, X., Wang, X., Chen, L., Huang, F., Yacoob, Y., et al. Hallusionbench: an advanced diagnostic suite for entangled language hallucination and visual illusion in large vision-language models. In *Proceedings of the IEEE/CVF Conference on Computer Vision and Pattern Recognition*, pp. 14375–14385, 2024.
- Gunjal, A., Yin, J., and Bas, E. Detecting and preventing hallucinations in large vision language models. In *Proceedings of the AAAI Conference on Artificial Intelligence*, volume 38, pp. 18135–18143, 2024.
- Han, Y., Zhang, C., Chen, X., Yang, X., Wang, Z., Yu, G., Fu, B., and Zhang, H. Chartllama: A multimodal llm for chart understanding and generation. *arXiv preprint arXiv:2311.16483*, 2023.
- He, K., Mao, R., Lin, Q., Ruan, Y., Lan, X., Feng, M., and Cambria, E. A survey of large language models for healthcare: from data, technology, and applications to accountability and ethics. *arXiv preprint arXiv:2310.05694*, 2023.
- Holtzman, A., Buys, J., Du, L., Forbes, M., and Choi, Y. The curious case of neural text degeneration. *arXiv preprint arXiv:1904.09751*, 2019.
- Huang, Q., Dong, X., Zhang, P., Wang, B., He, C., Wang, J., Lin, D., Zhang, W., and Yu, N. Opera: Alleviating hallucination in multi-modal large language models via over-trust penalty and retrospection-allocation. In *Proceedings of the IEEE/CVF Conference on Computer Vision and Pattern Recognition*, pp. 13418–13427, 2024.
- Jiang, C., Xu, H., Dong, M., Chen, J., Ye, W., Yan, M., Ye, Q., Zhang, J., Huang, F., and Zhang, S. Hallucination augmented contrastive learning for multimodal large language model. In *Proceedings of the IEEE/CVF Conference on Computer Vision and Pattern Recognition*, pp. 27036–27046, 2024.

- Kenton, J. D. M.-W. C. and Toutanova, L. K. Bert: Pre-training of deep bidirectional transformers for language understanding. In *Proceedings of naacL-HLT*, volume 1, pp. 2. Minneapolis, Minnesota, 2019.
- Leng, S., Zhang, H., Chen, G., Li, X., Lu, S., Miao, C., and Bing, L. Mitigating object hallucinations in large vision-language models through visual contrastive decoding. In *Proceedings of the IEEE/CVF Conference on Computer Vision and Pattern Recognition*, pp. 13872–13882, 2024.
- Li, C., Wong, C., Zhang, S., Usuyama, N., Liu, H., Yang, J., Naumann, T., Poon, H., and Gao, J. Llava-med: Training a large language-and-vision assistant for biomedicine in one day. *Advances in Neural Information Processing Systems*, 36, 2024a.
- Li, S., Cao, J., Ye, P., Ding, Y., Tu, C., and Chen, T. Clip-sam: Clip and sam collaboration for zero-shot anomaly segmentation. *arXiv preprint arXiv:2401.12665*, 2024b.
- Li, Y., Zhang, C., Yu, G., Yang, W., Wang, Z., Fu, B., Lin, G., Shen, C., Chen, L., and Wei, Y. Enhanced visual instruction tuning with synthesized image-dialogue data. In *Findings of the Association for Computational Linguistics ACL 2024*, pp. 14512–14531, 2024c.
- Liang, X., Yu, J., Mu, L., Zhuang, J., Hu, J., Yang, Y., Ye, J., Lu, L., Chen, J., and Hu, H. Mitigating hallucination in visual-language models via re-balancing contrastive decoding. In *Chinese Conference on Pattern Recognition and Computer Vision (PRCV)*, pp. 482–496. Springer, 2024.
- Lin, T.-Y., Maire, M., Belongie, S., Hays, J., Perona, P., Ramanan, D., Dollár, P., and Zitnick, C. L. Microsoft coco: Common objects in context. In *Computer Vision—ECCV 2014: 13th European Conference, Zurich, Switzerland, September 6-12, 2014, Proceedings, Part V 13*, pp. 740–755. Springer, 2014.
- Liu, F., Lin, K., Li, L., Wang, J., Yacoob, Y., and Wang, L. Mitigating hallucination in large multi-modal models via robust instruction tuning. In *The Twelfth International Conference on Learning Representations*, 2023.
- Liu, H., Li, C., Wu, Q., and Lee, Y. J. Visual instruction tuning. *Advances in neural information processing systems*, 36, 2024a.
- Liu, S., Zheng, K., and Chen, W. Paying more attention to image: A training-free method for alleviating hallucination in lvlms. *arXiv preprint arXiv:2407.21771*, 2024b.
- Ma, F., Jin, X., Wang, H., Xian, Y., Feng, J., and Yang, Y. Vista-llama: Reducing hallucination in video language models via equal distance to visual tokens. In *Proceedings of the IEEE/CVF Conference on Computer Vision and Pattern Recognition*, pp. 13151–13160, 2024.
- Rohrbach, A., Hendricks, L. A., Burns, K., Darrell, T., and Saenko, K. Object hallucination in image captioning. *arXiv preprint arXiv:1809.02156*, 2018.
- Shao, H., Hu, Y., Wang, L., Song, G., Waslander, S. L., Liu, Y., and Li, H. Lmdrive: Closed-loop end-to-end driving with large language models. In *Proceedings of the IEEE/CVF Conference on Computer Vision and Pattern Recognition*, pp. 15120–15130, 2024.
- Sun, Z., Shen, S., Cao, S., Liu, H., Li, C., Shen, Y., Gan, C., Gui, L.-Y., Wang, Y.-X., Yang, Y., et al. Aligning large multimodal models with factually augmented rlhf. *arXiv preprint arXiv:2309.14525*, 2023.
- Sutskever, I. Sequence to sequence learning with neural networks. *arXiv preprint arXiv:1409.3215*, 2014.
- Touvron, H., Lavril, T., Izacard, G., Martinet, X., Lachaux, M.-A., Lacroix, T., Rozière, B., Goyal, N., Hambro, E., Azhar, F., et al. Llama: Open and efficient foundation language models. *arXiv preprint arXiv:2302.13971*, 2023a.
- Touvron, H., Martin, L., Stone, K., Albert, P., Almahairi, A., Babaei, Y., Bashlykov, N., Batra, S., Bhargava, P., Bhosale, S., et al. Llama 2: Open foundation and fine-tuned chat models. *arXiv preprint arXiv:2307.09288*, 2023b.
- Wang, J., Wang, Y., Xu, G., Zhang, J., Gu, Y., Jia, H., Yan, M., Zhang, J., and Sang, J. An llm-free multi-dimensional benchmark for mllms hallucination evaluation. *arXiv preprint arXiv:2311.07397*, 2023a.
- Wang, L., He, J., Li, S., Liu, N., and Lim, E.-P. Mitigating fine-grained hallucination by fine-tuning large vision-language models with caption rewrites. In *International Conference on Multimedia Modeling*, pp. 32–45. Springer, 2024a.
- Wang, P., Bai, S., Tan, S., Wang, S., Fan, Z., Bai, J., Chen, K., Liu, X., Wang, J., Ge, W., et al. Qwen2-vl: Enhancing vision-language model’s perception of the world at any resolution. *arXiv preprint arXiv:2409.12191*, 2024b.
- Wang, S., Zhao, Z., Ouyang, X., Wang, Q., and Shen, D. Chatcad: Interactive computer-aided diagnosis on medical image using large language models. *arXiv preprint arXiv:2302.07257*, 2023b.
- Xiao, G., Tian, Y., Chen, B., Han, S., and Lewis, M. Efficient streaming language models with attention sinks. *arXiv preprint arXiv:2309.17453*, 2023.
- Xing, Y., Li, Y., Laptev, I., and Lu, S. Mitigating object hallucination via concentric causal attention. In *The Thirty-eighth Annual Conference on Neural Information Processing Systems*, 2024.

- Yang, Z., Liu, W., Gao, B., Xie, T., Li, Y., Ouyang, W., Poria, S., Cambria, E., and Zhou, D. Moose-chem: Large language models for rediscovering unseen chemistry scientific hypotheses. *arXiv preprint arXiv:2410.07076*, 2024.
- Ye, Q., Xu, H., Ye, J., Yan, M., Hu, A., Liu, H., Qian, Q., Zhang, J., and Huang, F. mplug-owl2: Revolutionizing multi-modal large language model with modality collaboration. In *Proceedings of the IEEE/CVF Conference on Computer Vision and Pattern Recognition*, pp. 13040–13051, 2024.
- Yin, S., Fu, C., Zhao, S., Xu, T., Wang, H., Sui, D., Shen, Y., Li, K., Sun, X., and Chen, E. Woodpecker: Hallucination correction for multimodal large language models. *arXiv preprint arXiv:2310.16045*, 2023.
- Yin, Z., Wang, J., Cao, J., Shi, Z., Liu, D., Li, M., Huang, X., Wang, Z., Sheng, L., Bai, L., et al. Lamm: Language-assisted multi-modal instruction-tuning dataset, framework, and benchmark. *Advances in Neural Information Processing Systems*, 36, 2024.
- Yu, T., Yao, Y., Zhang, H., He, T., Han, Y., Cui, G., Hu, J., Liu, Z., Zheng, H.-T., Sun, M., et al. Rlhf-v: Towards trustworthy mllms via behavior alignment from fine-grained correctional human feedback. In *Proceedings of the IEEE/CVF Conference on Computer Vision and Pattern Recognition*, pp. 13807–13816, 2024.
- Yue, Z., Zhang, L., and Jin, Q. Less is more: Mitigating multimodal hallucination from an eos decision perspective. *arXiv preprint arXiv:2402.14545*, 2024.
- Zhai, B., Yang, S., Xu, C., Shen, S., Keutzer, K., and Li, M. Halle-switch: Controlling object hallucination in large vision language models. *arXiv e-prints*, pp. arXiv–2310, 2023.
- Zhou, Y., Cui, C., Yoon, J., Zhang, L., Deng, Z., Finn, C., Bansal, M., and Yao, H. Analyzing and mitigating object hallucination in large vision-language models. *arXiv preprint arXiv:2310.00754*, 2023a.
- Zhou, Y., Cui, C., Yoon, J., Zhang, L., Deng, Z., Finn, C., Bansal, M., and Yao, H. Analyzing and mitigating object hallucination in large vision-language models. *arXiv preprint arXiv:2310.00754*, 2023b.
- Zhu, D., Chen, J., Shen, X., Li, X., and Elhoseiny, M. Minigpt-4: Enhancing vision-language understanding with advanced large language models. *arXiv preprint arXiv:2304.10592*, 2023.

A. More Experimental Results

A.1. CHAIR Benchmark

In this section, we provide more comparative performances on the CHAIR benchmark. Specifically, we apply our proposed AttnReal approach to various MLLMs (including LaVA-1.5-13B, MiniGPT-4, Shikra, mPLUG-Owl2, and Qwen2-VL) and decoding strategies using different down-scaling factors α and compare the performance with existing training-free methods designed for mitigating MLLM hallucinations. The results are illustrated in Figures 6 to 10. After applying AttnReal, hallucinations of the model are significantly reduced and an increase in the F1 score can be obtained under a wide range of values of α in most settings. Compared to existing methods, AttnReal achieves better performance on most models and decoding approaches, yielding results that outperform the state-of-the-art methods on both CHAIR metrics and the F1 score. These experimental results further validate the wide applicability of AttnReal on MLLMs of different scales and structures.

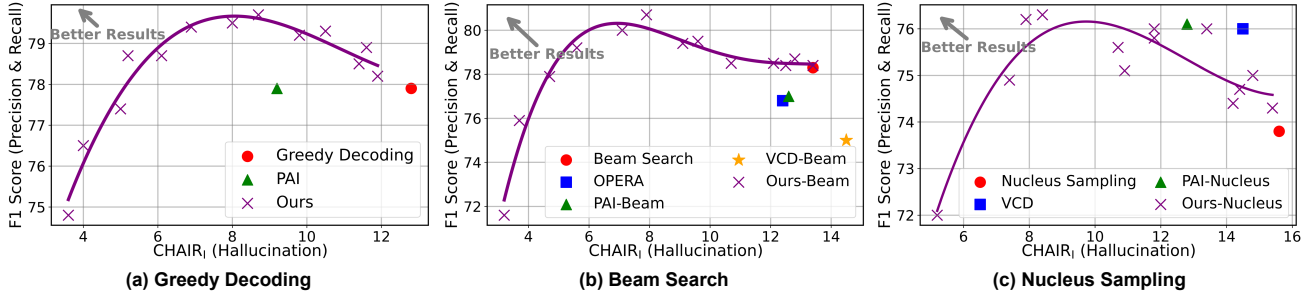


Figure 6: Performance comparison for various training-free methods to mitigate MLLM hallucinations on LLaVA-1.5-13B and the CHAIR benchmark using three decoding strategies. Lower CHAIR₁ represents fewer hallucinations. Higher F1 scores mean better overall performance of the responses. The curve in each sub-figure is obtained by adjusting the intensity of AttnReal.

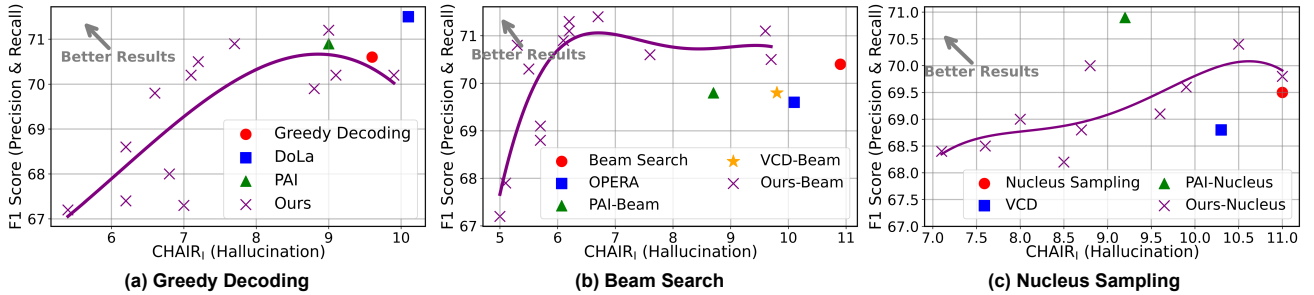


Figure 7: Performance comparison for various training-free methods to mitigate MLLM hallucinations on MiniGPT-4 and the CHAIR benchmark using three decoding strategies. Lower CHAIR₁ represents fewer hallucinations. Higher F1 scores mean better overall performance of the responses. The curve in each sub-figure is obtained by adjusting the intensity of AttnReal.

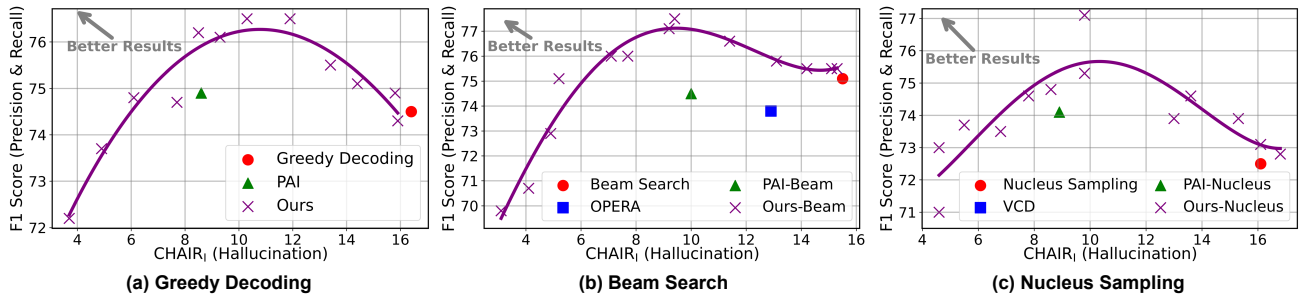


Figure 8: Performance comparison for various training-free methods to mitigate MLLM hallucinations on Shikra and the CHAIR benchmark using three decoding strategies. Lower CHAIR₁ represents fewer hallucinations. Higher F1 scores mean better overall performance of the responses. The curve in each sub-figure is obtained by adjusting the intensity of AttnReal.

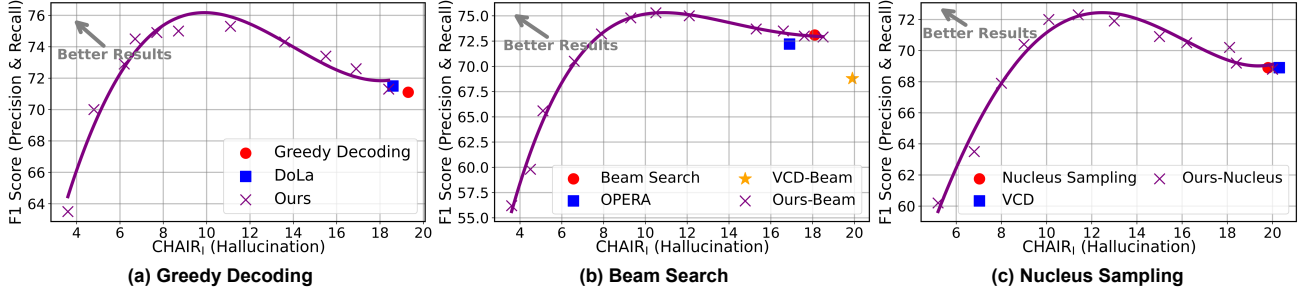


Figure 9: Performance comparison for various training-free methods to mitigate MLLM hallucinations on mPLUG-Owl2 and the CHAIR benchmark using three decoding strategies. Lower CHAIR₁ represents fewer hallucinations. Higher F1 scores mean better overall performance of the responses. The curve in each sub-figure is obtained by adjusting the intensity of AttnReal.

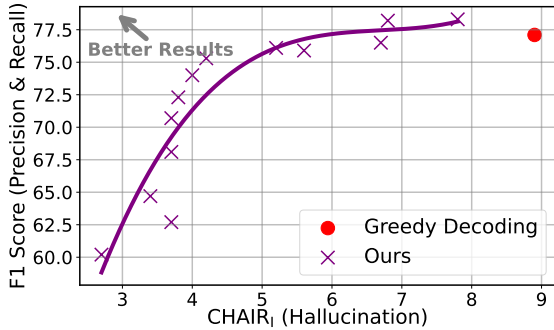


Figure 10: Performance comparison for AttnReal and the baseline Greedy Decoding on Qwen2-VL and the CHAIR benchmark.

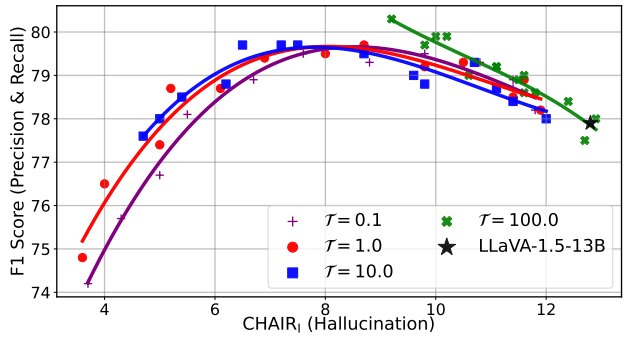


Figure 11: Ablation study on LLaVA-1.5-13B about the effect of different sink thresholds \mathcal{T} on the performance.

A.2. Ablation Study about Attention Sink Threshold \mathcal{T} on Larger Model

To explore the robustness of AttnReal to the attention sink threshold \mathcal{T} , we choose LLaVA-1.5-13B, which is of larger scale than LLaVA-1.5-7B explored in Section 4.3, for further validation. As can be concluded from Figure 11, although the values of \mathcal{T} vary considerably, i.e., $\mathcal{T} = [0.1, 1, 10, 100]$, the results of different settings fall on similar trajectories as the intensity of AttnReal enhances and hallucinations decrease. Specifically, at lower AttnReal intensities, hallucinations are reduced from baseline, and F1 scores are improved because of the significant increase in precision. When the AttnReal intensity becomes higher, the hallucinations continue to decrease, but the F1 score decreases because the precision cannot be further improved, and the model discards uncertain contents, resulting in lower recall. This supplementary ablation study demonstrates that AttnReal is also robust to attention sink threshold settings on larger models.

A.3. Ablation Study about Random Seeds

To mitigate the potential influence of random image subset sampling on the results of the CHAIR benchmark and to further validate the robustness of our proposed AttnReal method, we conduct additional experiments using two different random seeds, distinct from the one used in the main manuscript. Specifically, we select LLaVA-1.5-7B and LLaVA-1.5-13B as representative models of different model scales, as most of the comparative methods have been implemented on these models. We apply our proposed AttnReal to these models using different down-scaling factors α and compare the performance with existing training-free methods. Figures 12 and 13 show the comparative results using the first additional random seed, and Figures 14 and 15 demonstrate the results using the second random seed. As can be concluded, AttnReal consistently achieves an excellent trade-off between hallucination and F1 score and can yield superior results to state-of-the-art methods on different decoding strategies using both additional random seeds. This consistency confirms that the effectiveness of AttnReal is not contingent on specific samples, thereby strengthening the robustness of our proposed method.

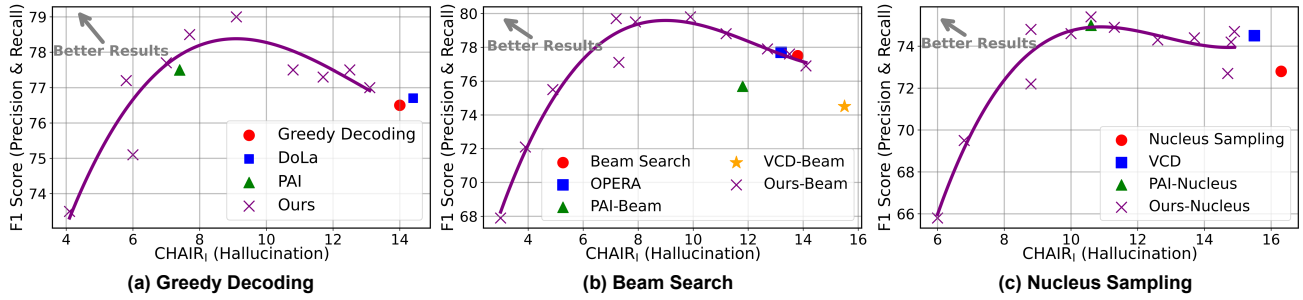


Figure 12: Ablation study on LLaVA-1.5-7B using different random seeds ($seed = 48$).

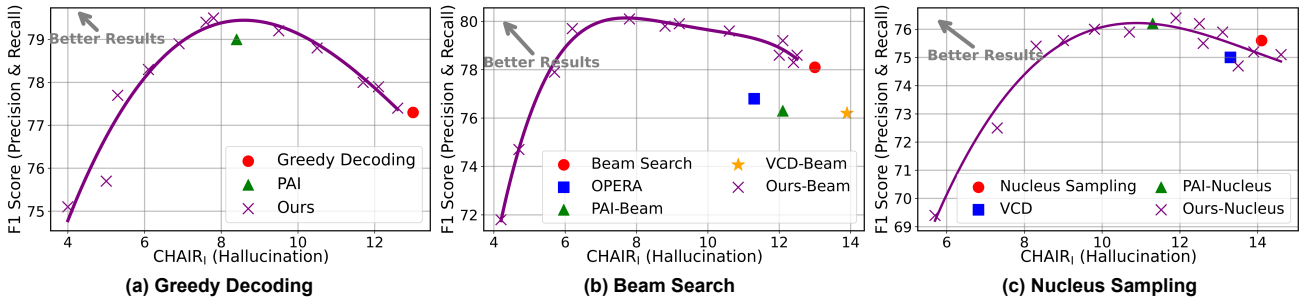


Figure 13: Ablation study on LLaVA-1.5-13B using different random seeds ($seed = 48$).

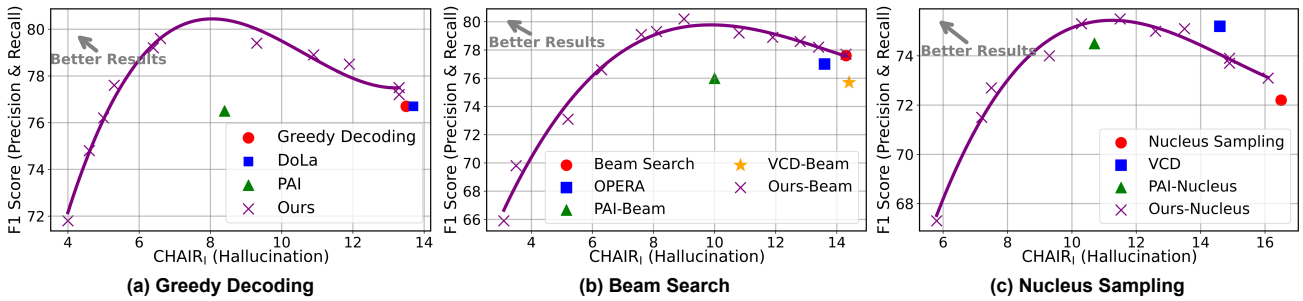


Figure 14: Ablation study on LLaVA-1.5-7B using different random seeds ($seed = 104$).

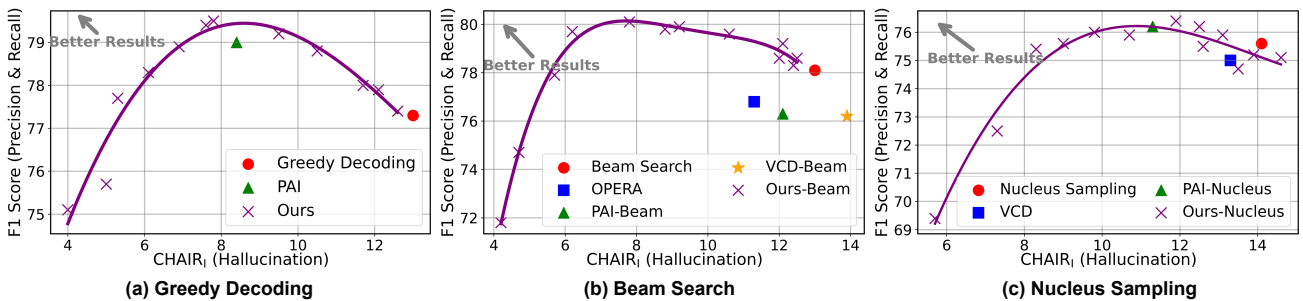


Figure 15: Ablation study on LLaVA-1.5-13B using different random seeds ($seed = 104$).

A.4. AMBER Benchmark

AMBER (An LLM-free Multi-dimensional Benchmark) (Wang et al., 2023a) introduces a comprehensive LLM-free framework for assessing hallucinations in MLLMs across diverse dimensions. The benchmark consists of 1004 samples and supports the evaluation of generative and discriminative tasks, and we focus on the generative evaluation. AMBER employs four metrics for evaluating hallucinations on generative tasks: *CHAIR*, *Cover*, *Hal*, and *Cog*. Similar to CHAIR (Rohrbach et al., 2018), AMBER compares the mentioned objects by MLLMs and the annotated object lists and calculates *CHAIR* and *Cover* scores:

$$CHAIR = 1 - \frac{|\{\text{correct mentioned objects}\}|}{|\{\text{all mentioned objects}\}|}, \quad Cover = \frac{|\{\text{correct mentioned objects}\}|}{|\{\text{ground-truth objects}\}|} \quad (7)$$

Besides, *Hal* reflects the proportion of hallucinated responses from all samples. *Cog* assesses how similar the hallucinations are to those in human cognition by comparing the mentioned objects by MLLMs and a set of human-curated hallucinatory target objects:

$$Cog = \frac{|\{\text{hallucinated target objects}\}|}{|\{\text{all mentioned objects}\}|} \quad (8)$$

We evaluate our proposed AttnReal on the AMBER benchmark and various open-source MLLMs and decoding strategies. As can be seen in Table 5, our proposed AttnReal achieves the best hallucination performance (including CHAIR, Hal, and Cog metrics) across most model and decoding strategy settings, which demonstrates the effectiveness and wide applicability of AttnReal. Meanwhile, AttnReal yields comparable or superior Cover scores compared to baselines on most models, indicating that AttnReal can improve the overall performance of MLLMs beyond response faithfulness.

Table 5: AMBER generative evaluation results on five open-source MLLMs. For CHAIR, Hal and Cog, lower values mean better performance. For Cover, high values mean better performance. The best results are **bolded**, and the suboptimal results are underlined. “-” means the corresponding method is not implemented in this model.

Methods	Decoding Strategy	LLaVA-1.5-7B				LLaVA-1.5-13B				MiniGPT-4			
		CHAIR↓	Cover↑	Hal↓	Cog↓	CHAIR↓	Cover↑	Hal↓	Cog↓	CHAIR↓	Cover↑	Hal↓	Cog↓
Greedy	Greedy Decoding	6.1	<u>51.1</u>	28.9	3.1	6.2	51.0	28.9	3.0	15.1	62.6	62.8	10.3
DoLa (Chuang et al., 2023)		6.3	<u>51.1</u>	29.2	3.1	-	-	-	-	16.0	62.6	63.4	11.0
PAI (Liu et al., 2024b)		<u>4.5</u>	47.2	<u>21.0</u>	1.4	4.8	<u>51.5</u>	<u>26.3</u>	<u>1.6</u>	<u>10.7</u>	<u>59.3</u>	<u>43.0</u>	<u>5.6</u>
Ours		3.2	51.2	19.2	<u>1.5</u>	3.2	51.9	18.9	1.5	10.3	56.7	41.7	5.2
Beam Search	Beam Search	7.4	<u>49.4</u>	30.9	3.6	7.2	<u>49.5</u>	30.8	3.6	14.1	<u>61.0</u>	60.1	9.1
OPERA (Huang et al., 2024)		6.4	48.9	27.7	3.0	<u>6.1</u>	48.1	<u>24.8</u>	<u>2.7</u>	12.3	57.7	48.1	6.4
VCD-Beam (Leng et al., 2024)		7.5	51.2	33.5	3.3	7.5	50.3	32.6	3.0	15.4	61.5	61.8	9.4
PAI-Beam (Liu et al., 2024b)		7.2	45.3	<u>27.6</u>	<u>2.4</u>	6.2	47.6	26.9	1.8	<u>10.1</u>	55.2	<u>36.2</u>	<u>4.7</u>
Ours	4.1	48.6	21.6	1.8	4.2	48.0	20.8	1.8	7.8	55.7	34.6	3.9	
Nucleus Sampling	Nucleus Sampling	9.0	50.6	40.4	3.6	8.6	49.6	38.4	3.6	15.5	<u>60.2</u>	63.5	9.4
VCD (Leng et al., 2024)		7.3	<u>50.2</u>	33.8	<u>3.1</u>	7.3	50.7	32.6	3.3	15.3	60.9	61.7	9.6
PAI-Nucleus (Liu et al., 2024b)		<u>6.6</u>	49.2	31.1	2.2	<u>6.6</u>	<u>50.6</u>	<u>31.3</u>	<u>2.2</u>	<u>11.3</u>	57.4	<u>43.8</u>	<u>5.8</u>
Ours		6.4	48.2	<u>31.9</u>	2.2	5.4	50.3	29.0	1.9	10.4	54.7	42.0	4.4

Methods	Decoding Strategy	Shikra				mPLUG-Owl2			
		CHAIR↓	Cover↑	Hal↓	Cog↓	CHAIR↓	Cover↑	Hal↓	Cog↓
Greedy	Greedy Decoding	11.0	50.9	48.2	5.2	<u>9.9</u>	<u>51.5</u>	40.3	<u>5.0</u>
DoLa (Chuang et al., 2023)		-	-	-	-	10.3	51.4	42.4	5.2
PAI (Liu et al., 2024b)		<u>6.5</u>	49.0	<u>32.4</u>	<u>2.3</u>	-	-	-	-
Ours		5.2	<u>49.6</u>	27.9	2.1	5.4	52.0	26.2	2.2
Beam Search	Beam Search	10.7	50.9	47.7	5.8	11.5	49.3	42.3	5.3
OPERA (Huang et al., 2024)		9.5	<u>50.1</u>	41.2	4.5	<u>10.1</u>	49.0	<u>36.9</u>	<u>4.1</u>
VCD-Beam (Leng et al., 2024)		-	-	-	-	11.5	51.2	45.4	5.0
PAI-Beam (Liu et al., 2024b)		<u>7.2</u>	47.5	<u>30.8</u>	<u>2.8</u>	-	-	-	-
Ours	4.8	48.0	25.0	1.9	6.8	<u>49.8</u>	26.5	2.6	
Nucleus Sampling	Nucleus Sampling	11.7	51.8	53.5	5.7	13.0	50.3	50.0	5.4
VCD (Leng et al., 2024)		-	-	-	-	<u>11.5</u>	<u>51.3</u>	<u>45.7</u>	<u>4.9</u>
PAI-Nucleus (Liu et al., 2024b)		<u>7.0</u>	49.1	<u>33.0</u>	2.4	-	-	-	-
Ours		5.4	<u>50.5</u>	29.8	<u>2.5</u>	9.4	51.8	40.7	3.2

A.5. MMHal-Bench

In this section, the results of more MLLMs on MMHal-Bench are demonstrated in Figures 16 to 19. On all models, our proposed AttnReal method achieves the highest overall scores and substantially improves response faithfulness, demonstrating the comprehensive capability of our AttnReal method on various hallucination types.

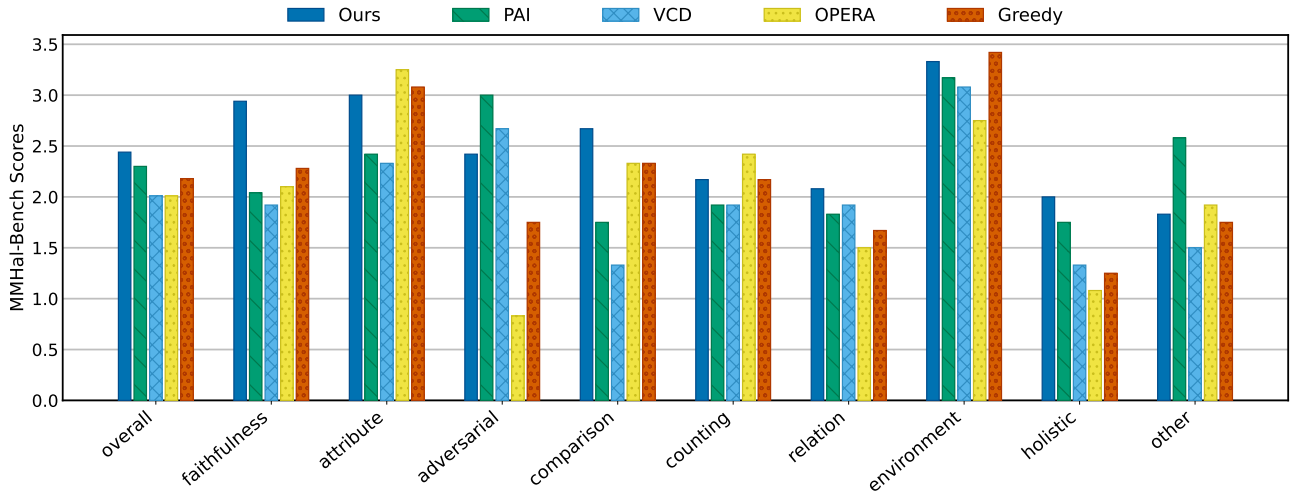


Figure 16: Comparative results on the MMHal-Bench and LLaVA-1.5-13B. To all metrics, higher scores mean better performance.

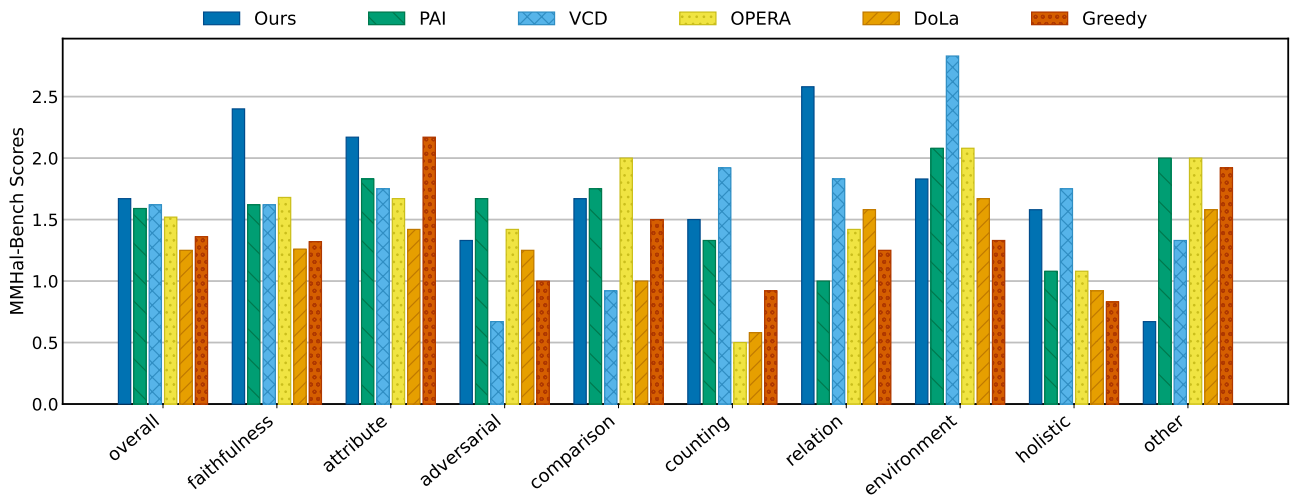


Figure 17: Comparative results on the MMHal-Bench and MiniGPT-4. To all metrics, higher scores mean better performance.

Attention Reallocation: Towards Zero-cost and Controllable Hallucination Mitigation of MLLMs

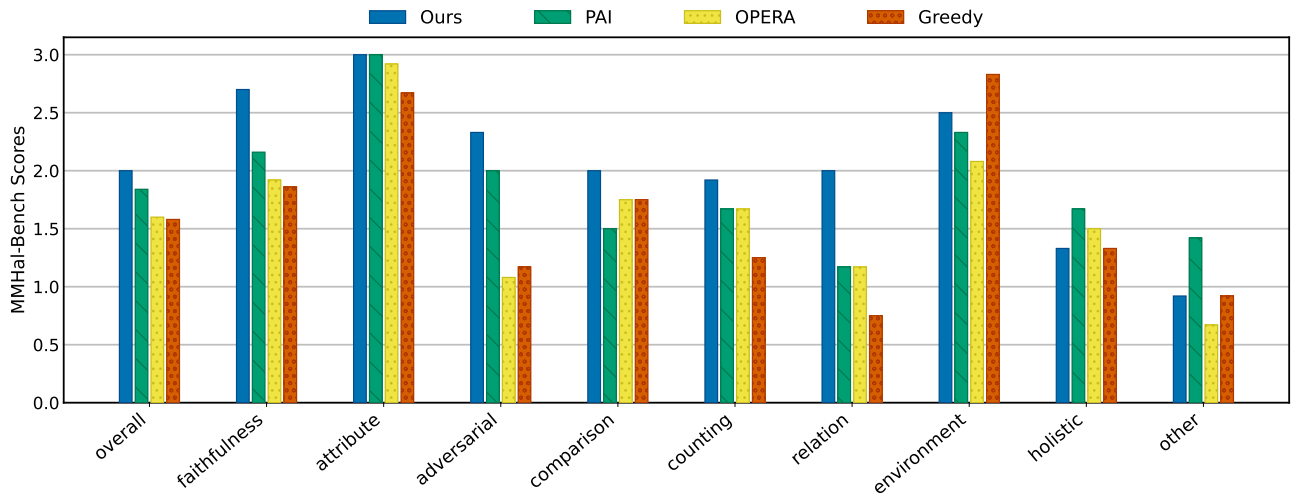


Figure 18: Comparative results on the MMHal-Bench and Shikra. To all metrics, higher scores mean better performance.

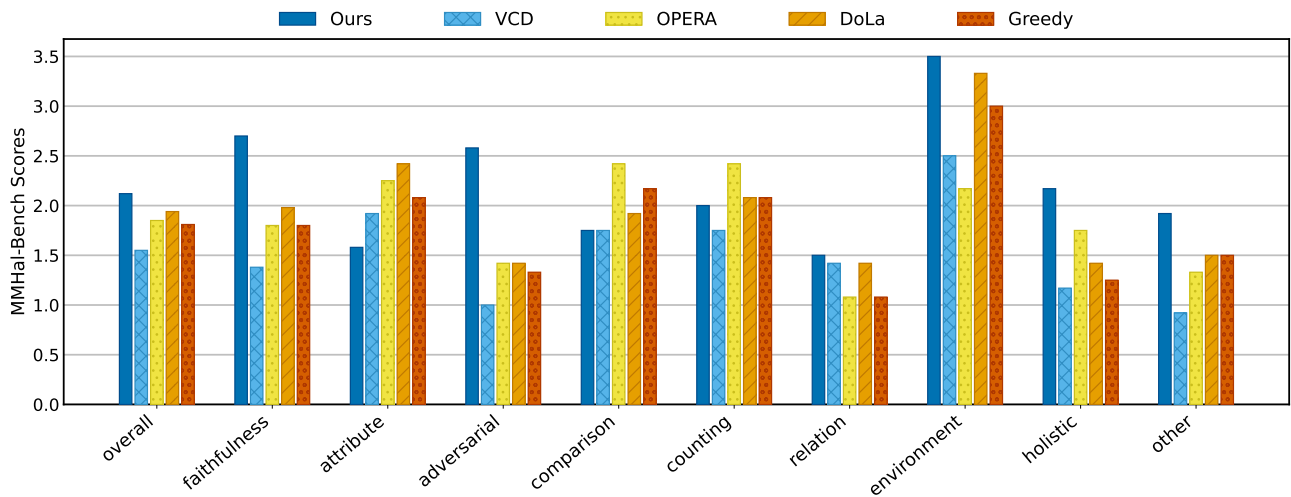


Figure 19: Comparative results on the MMHal-Bench and mPLUG-Owl2. To all metrics, higher scores mean better performance.

B. Qualitative Study

In this section, we show the qualitative results of AttnReal eliminating the hallucinations of multiple MLLMs. Specifically, the hallucinated responses of the MLLMs and the corrected responses when applying AttnReal are provided, as well as the input images. Figures 20 to 25 correspond to LaVA-1.5-7B (Liu et al., 2024a), LLaVA-1.5-13B (Liu et al., 2024a), MiniGPT-4 (Zhu et al., 2023), Shikra (Chen et al., 2023), mPLUG-Owl2 (Ye et al., 2024), and Qwen2-VL (Wang et al., 2024b), respectively, with three cases for each model. Hallucinations in the responses are highlighted in red. From the results, we can conclude that the responses of MLLMs are more faithful and more focused on the image contents using AttnReal.

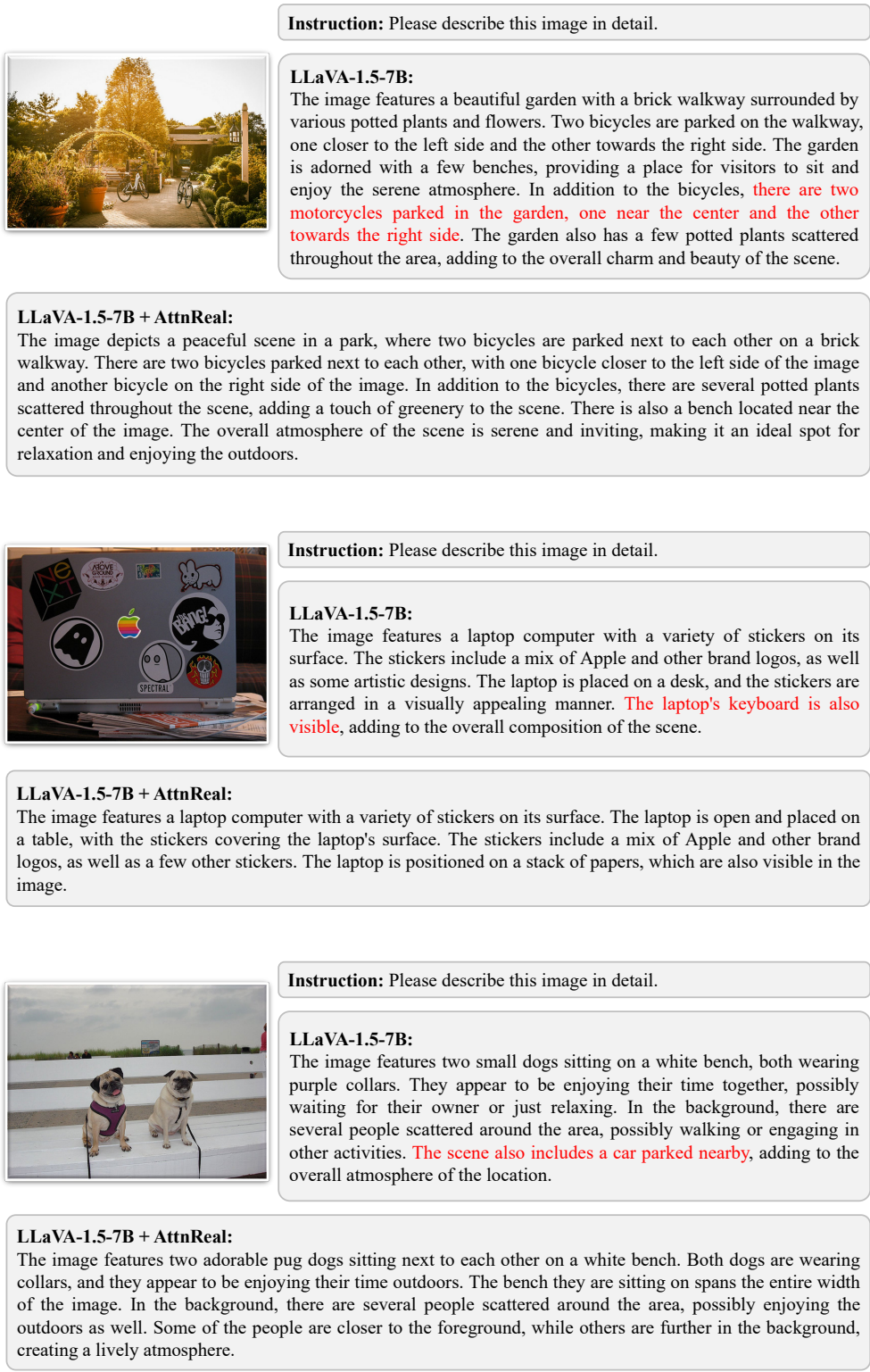


Figure 20: Qualitative results of the hallucination mitigation effect of our proposed AttnReal on the LLaVA-1.5-7B model. Hallucinations in the responses are highlighted in red.



Instruction: Please describe this image in detail.

LLaVA-1.5-13B:

The image features a young baseball player standing on a field, wearing a baseball uniform and a baseball glove. He appears to be a catcher, as he is positioned in the outfield, ready to catch a ball. The player is looking at the camera, possibly posing for a picture. In the background, **there is a car parked near the field, and a truck can be seen further away.** The scene also includes **a bench located near the edge of the field,** possibly for players to rest or sit during the game.

LLaVA-1.5-13B + AttnReal:

The image features a young baseball player standing on a field, wearing a baseball uniform and a baseball glove. The player is positioned in the center of the field, holding a baseball glove in his hand. The scene appears to be a baseball field, with a fence visible in the background. The baseball player is likely preparing to catch a ball or practice his skills.



Instruction: Please describe this image in detail.

LLaVA-1.5-13B:

The image features a cozy bedroom with a large window that allows natural light to flood the space. The bed is positioned in the center of the room, with a white comforter covering it. The window is open, providing a view of the outdoors and allowing fresh air to circulate. In addition to the bed, **there is a chair located near the right side of the room, and a clock can be seen on the wall above it.** A small vase is also present in the room, adding a touch of decoration to the space.

LLaVA-1.5-13B + AttnReal:

The image depicts a cozy bedroom scene with a large bed occupying most of the space in the room. The bed is positioned in front of a large window, allowing natural light to fill the room. The bed is covered with a white comforter, creating a comfortable and inviting atmosphere in the bedroom.



Instruction: Please describe this image in detail.

LLaVA-1.5-13B:

The image features a bathroom with a glass shower door, which is open, revealing a walk-in shower. The shower has a tile floor and a glass door, giving it a modern and sleek appearance. A toilet is located to the left of the shower, and **a sink can be seen in the background.** There are two towels hanging on the wall, one on the left side and the other on the right side of the shower. **The towels are placed at different heights,** with the one on the left being higher and the one on the right being lower.

LLaVA-1.5-13B + AttnReal:

The image depicts a modern bathroom featuring a walk-in shower with a glass door. The shower has a tiled floor and walls, giving the bathroom a clean and elegant appearance. There are two towels hanging on a towel rack next to the shower. The bathroom also features a toilet located to the left of the shower. The bathroom appears to be well-maintained and ready for use.

Figure 21: Qualitative results of the hallucination mitigation effect of our proposed AttnReal on the LLaVA-1.5-13B model. Hallucinations in the responses are highlighted in red.



Instruction: Please describe this image in detail.

MiniGPT-4:

This image shows a plate of food on a table. The plate has a piece of white rice on it, and there are also some broccoli and chicken on top of the rice. The broccoli is cut into small pieces and is covered in a sauce, while the chicken is sliced into thin pieces. The plate is on a dark-colored table, and **there is a fork and knife next to it**. The lighting in the image is bright and even, with no shadows or highlights. The overall mood of the image is casual and relaxed.

MiniGPT-4 + AttnReal:

This image shows a plate of food consisting of rice, broccoli, and chicken. The food is served on a white plate and appears to be well-cooked and appetizing. The plate is placed on a dark-colored table, which provides a contrasting background for the food. The image is well-lit, with the light source coming from the top of the frame. The lighting creates a warm and inviting atmosphere for the dish. Overall, the image is visually appealing and appetizing.



Instruction: Please describe this image in detail.

MiniGPT-4:

This image shows a city street at sunset, with tall buildings in the background. The buildings are made of brick and have many windows and balconies. The street is lined with trees and **there are cars driving on it**. The sky is cloudy and there is a red traffic light at the end of the street.

MiniGPT-4 + AttnReal:

The image shows a cityscape at sunset, with tall buildings in the background and a traffic light in the foreground. The buildings are made of concrete and steel, with many windows and balconies. The sky is cloudy and the sun is setting behind the buildings, casting a warm orange light on the street. There are no people or cars in the image.



Instruction: Please describe this image in detail.

MiniGPT-4:

The image shows a group of trains parked on a railroad track in front of a large building. The building appears to be a warehouse or industrial facility, with several large metal doors **and windows** on the side facing the tracks. The trains are parked in a line, with several cars **and trucks** parked next to them. The tracks appear to be used for freight or passenger trains, as there are several other trains parked nearby. The sky is overcast, **with a few clouds visible in the distance**.

MiniGPT-4 + AttnReal:

This image shows a group of trains parked on a railroad track in front of a large building. The building appears to be a warehouse or storage facility, and there are several cars parked next to the tracks. The trains are painted in different colors, including blue, yellow, and white, and they are all parked facing the same direction. There are trees and other vegetation in the background, and the sky appears to be overcast.

Figure 22: Qualitative results of the hallucination mitigation effect of our proposed AttnReal on the MiniGPT-4 model. Hallucinations in the responses are highlighted in red.



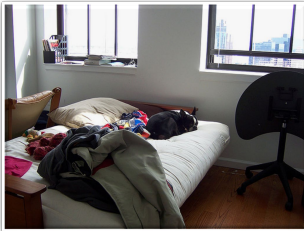
Instruction: Please describe this image in detail.

Shikra:

The image features a group of three zebras standing in a dry, barren field. Two of the zebras are standing close together, while the third one is slightly further away. They appear to be the main focus of the scene, occupying a significant portion of the image. In addition to the zebras, **there are also several birds scattered throughout the field**, creating a lively atmosphere. **Some of the birds are found near the zebras**, while others are further away, adding a sense of depth to the landscape.

Shikra + AttnReal:

The image features a group of three zebras standing in a dry grass-covered field. Two of the zebras are standing close to each other, while the third one is slightly further away. They appear to be enjoying the sunny day and each other's company. The field is filled with tall, dry grass, creating a unique environment for the zebras. There are trees visible in the background, adding some greenery to the scene. Overall, the image captures a moment of peace and tranquility as the zebras graze and interact in their natural habitat.



Instruction: Please describe this image in detail.

Shikra:

The image depicts a black dog lying down on a bed in a messy bedroom. The bed is covered with **a white comforter** and several blankets, giving the dog a comfortable spot to rest. The room appears to be in disarray with clothes scattered all over the floor and on the bed. There is a chair near the foot of the bed, and a desk is situated towards the left side of the room. **A bottle can be seen placed on the bed**, possibly for the dog to drink from while resting. Additionally, **a handbag is located near the edge of the bed**.

Shikra + AttnReal:

The image depicts a black dog lying down on a bed in a messy bedroom. The bed, which occupies a significant portion of the room, is covered with clothes and blankets. The dog is comfortably sleeping on the bed. In addition to the bed, there is a desk and a chair in the room, both of which contribute to the overall cluttered appearance of the room. The bed is positioned near a window, allowing natural light to illuminate the space.



Instruction: Please describe this image in detail.

Shikra:

The image depicts a lively street scene featuring a large building with multiple windows adorned with banners and flags. The storefront of the building has a unique architectural design, and it is situated next to a few other buildings. There are several bicycles parked in front of the building, which could be a popular spot for biking enthusiasts to visit the pizzeria. In addition to the bicycles, **there are a few people walking around the area, possibly pedestrians or customers of the pizzeria**. The presence of these individuals adds to the vibrant atmosphere along the street.

Shikra + AttnReal:

The image depicts a lively street scene featuring a large pizza restaurant with a tall building situated next to a few other buildings. There are multiple bicycles parked in front of the pizzeria, which suggests that it is a popular and well-established business. In the foreground, there are several bicycles parked in front of the building, indicating that the area is bustling with activity. The street appears to be a busy and lively urban setting.

Figure 23: Qualitative results of the hallucination mitigation effect of our proposed AttnReal on the Shikra model. Hallucinations in the responses are highlighted in red.

Instruction: Please describe this image in detail.



mPLUG-Owl2:

The image features a blue and yellow train traveling down the tracks, passing through a city. The train is quite long, occupying a significant portion of the scene. There are several buildings visible in the background, with some located on the left side of the train and others on the right. In addition to the train, **there are a few people scattered around the scene. One person is standing near the left side of the train, while another person is located closer to the center. A third person can be seen on the right side of the train.**

mPLUG-Owl2 + AttnReal:

The image features a blue and yellow train traveling down the railroad tracks. The train occupies a significant portion of the scene, stretching from the left to the right side of the image. The train appears to be a passenger train, as indicated by the presence of multiple windows along its length. In addition to the train, there are several buildings visible in the background, adding to the urban atmosphere of the scene.

Instruction: Please describe this image in detail.



mPLUG-Owl2:

The image features a small model of a lighthouse, placed in a garden setting. The lighthouse is made of wood and has a brown color, giving it a rustic appearance. It stands tall in the garden, surrounded by various plants and trees. In the background, **there are several potted plants, some of which are located near the lighthouse, while others are scattered throughout the garden.** A few people can be seen in the scene, possibly admiring the model lighthouse or enjoying the garden's ambiance. Additionally, **there are two benches in the garden, one near the left side and another closer to the right side.** The benches provide a place for visitors to sit and relax while appreciating the garden's beauty.

mPLUG-Owl2 + AttnReal:

The image features a small model of a lighthouse in a garden setting. The lighthouse is made of wood and is surrounded by trees. There are several people visible in the scene, possibly admiring the model lighthouse. The lighthouse appears to be made of clay, giving it an old-fashioned appearance. In addition to the lighthouse, there is also a train set in the scene, adding to the overall charm of the scene. The model lighthouse is surrounded by trees, creating a serene and peaceful atmosphere.

Instruction: Please describe this image in detail.



mPLUG-Owl2:

The image features a stop sign with a four-way sign on top, located near a street. The stop sign is prominently displayed, with the four-way sign positioned above it. The four-way sign is slightly obscured by the stop sign, but it is still visible. In the background, there are trees, adding a touch of nature to the scene. **A car can be seen parked on the street, and a person is standing nearby, possibly waiting to cross the street or observing the traffic.**

mPLUG-Owl2 + AttnReal:

The image features a four-way stop sign that has been vandalized with red spray paint. The stop sign is prominently displayed in the center of the scene, surrounded by trees and houses in the background. The graffiti on the stop sign adds an element of urban decay to the otherwise peaceful scene.

Figure 24: Qualitative results of the hallucination mitigation effect of our proposed AttnReal on the mPLUG-Owl2 model. Hallucinations in the responses are highlighted in red.

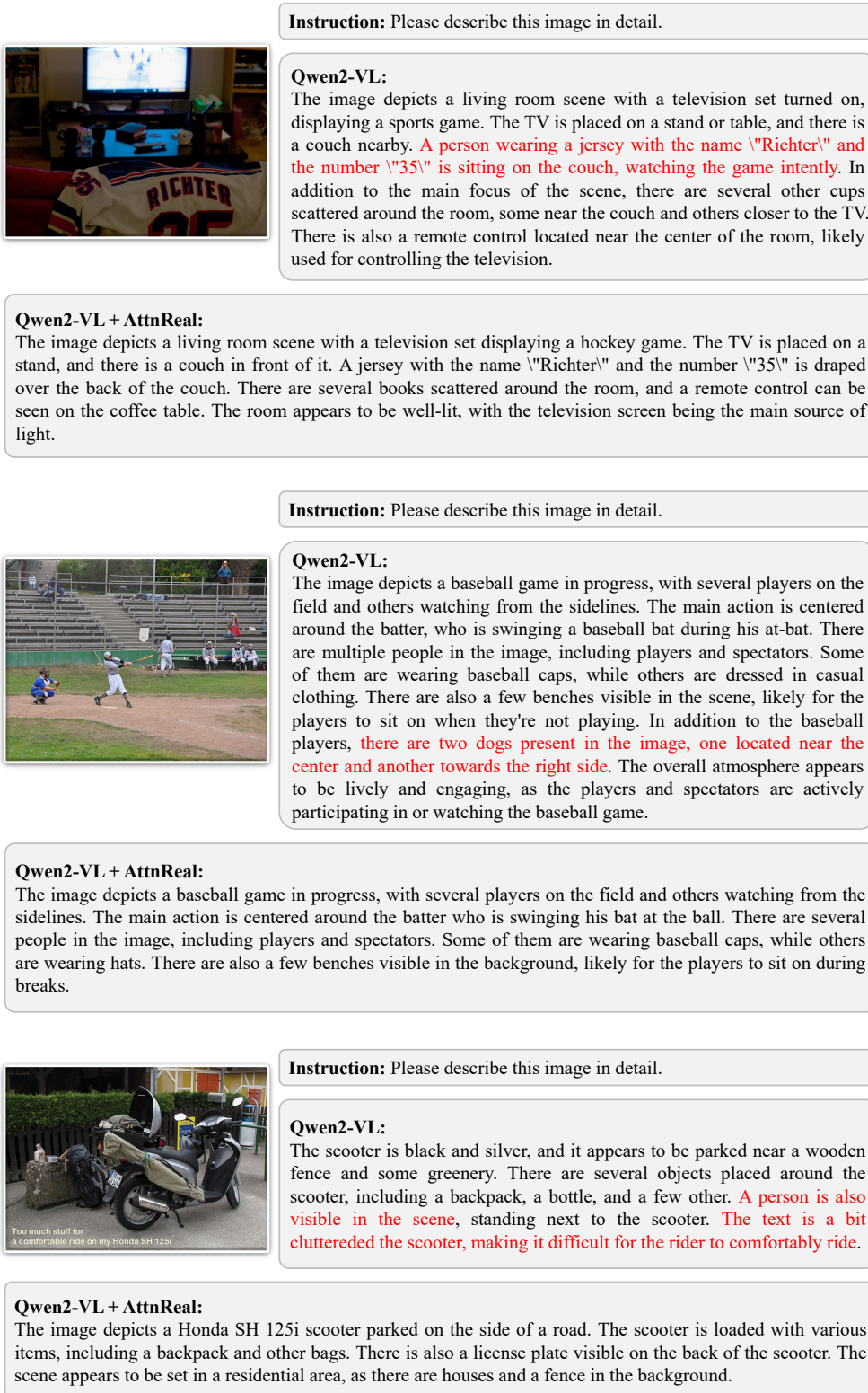


Figure 25: Qualitative results of the hallucination mitigation effect of our proposed AttnReal on the Qwen2-VL model. Hallucinations in the responses are highlighted in red.

C. GPT-assisted Evaluation Prompt

We provide the prompt used for GPT-assisted evaluation in Table 6, which is constructed based on the prompt used by PAI (Liu et al., 2024b). Specifically, we follow MMHal-Bench (Sun et al., 2023) to specify the criterion for each rating in the prompt to conduct a fairer evaluation of multiple MLLMs and methods.

Table 6: Prompt for GPT-4o assisted evaluation.

GPT-4o Assisted Evaluation
<p>You are required to score the performance of an AI assistant in describing a given image. Please pay extra attention to hallucination, which refers to the part of descriptions that are inconsistent with the image content, such as claiming the existence of something not present in the image or describing incorrectly in terms of the counts, positions, or colors of objects in the image. Please rate the response of the assistant on a scale of 1 to 5, where a higher score indicates better performance, according to the following criteria:</p> <p>Correctness</p> <ul style="list-style-type: none"> 5 - The response is entirely correct, with no hallucinations. 4 - The response is mostly correct, with only minor inaccuracies that do not significantly alter the meaning. 3 - The response contains some inaccuracies, but they are not critical to understanding the main content. 2 - The response has multiple inaccuracies that affect the correctness. 1 - The response is largely incorrect, with significant hallucinations. <p>Detailedness</p> <ul style="list-style-type: none"> 5 - The response is rich in necessary details, covering all important aspects of the image without irrelevant information. 4 - The response provides a good level of detail, but misses a minor aspect. 3 - The response includes some details but misses multiple important aspects. 2 - The response is lacking in important details and is vague. 1 - The response provides minimal detail and lacks depth. <p>Please output two scores for the AI assistant, indicating the ratings for Correctness and Detailedness respectively. Following the scores, please provide an explanation of your evaluation.</p> <p>[Assistant Response] {response} [End of Assistant Response]</p> <p>Output format: Correctness: <Score 1> Detailedness: <Score 2> Reason:</p>

D. Algorithm of Attention Reallocation

In this section, we provide the algorithm of our proposed Attention Reallocation (AttnReal) approach.

Algorithm 1 Attention Reallocation Steps

- Input:** Post-softmax attention map of all token types $[A_s, A_v, A_i, A_o]$
- 1: **Identify Sinks:** Construct the attention sink set S_{sink} as Equation (4)
 - 2: **Recycle Attention:** Suppress A_o for tokens in S_{sink} as Equation (5)
 - 3: **Reallocate Attention:** Strengthen A_v as Equation (6)
- Output:** Updated attention map $[A_s, A'_v, A_i, A'_o]$